

 Open access • Posted Content • DOI:10.21203/RS.3.RS-101657/V1

Climate change signal in global agriculture emerges earlier in new generation of climate and crop models — [Source link](#)

Jonas Jaegermeyr, Christoph Müller, Alex C. Ruane, Joshua Elliott ...+34 more authors

Published on: 12 Aug 2021

Topics: Climate change and Agriculture

Related papers:

- [Global Climate Change and Agriculture](#)
- [Crop production and global climate change](#)
- [Global Climate Change: Effects on Agriculture](#)
- [Do Climate Signals Matter? Evidence from Agriculture](#)
- [Implications of Climate Change for Crop Production in Japan](#)

Share this paper:    

View more about this paper here: <https://typeset.io/papers/climate-change-signal-in-global-agriculture-emerges-earlier-4fbwwy8aa5>

Climate change signal in global agriculture emerges earlier in new generation of climate and crop models

Jonas Jaegermeyr (✉ jonas.jaegermeyr@columbia.edu)

Columbia University <https://orcid.org/0000-0002-8368-0018>

Christoph Müller

Potsdam Institute for Climate Impact Research <https://orcid.org/0000-0002-9491-3550>

Alex Ruane

NASA Goddard Institute for Space Studies <https://orcid.org/0000-0002-5582-9217>

Joshua Elliott

Columbia University

Juraj Balkovic

International Institute for Applied Systems Analysis (IIASA)

Oscar Castillo

University of Florida

Babacar Faye

Institut de recherche pour le développement

Ian Foster

University of Chicago

Christian Folberth

International Institute for Applied Systems Analysis <https://orcid.org/0000-0002-6738-5238>

James Franke

University of Chicago

Kathrin Fuchs

Karlsruhe Institute of Technology

Jose Guarin

Columbia University <https://orcid.org/0000-0002-3167-4329>

Jens Heinke

Potsdam Institute for Climate Impacts Research

Gerrit Hoogenboom

University of Florida <https://orcid.org/0000-0002-1555-0537>

Toshichika Iizumi

National Agriculture and Food Research Organization <https://orcid.org/0000-0002-0611-4637>

Atul Jain

University of Illinois at Urbana-Champaign <https://orcid.org/0000-0002-4051-3228>

David Kelly

University of Chicago

Nikolay Khabarov

International Institute for Applied Systems Analysis <https://orcid.org/0000-0001-5372-4668>

Stefan Lange

Potsdam Institute for Climate Impact Research (PIK), Member of the Leibniz Association

<https://orcid.org/0000-0003-2102-8873>

Tzu-Shun Lin

University of Illinois at Urbana-Champaign

Wenfeng Liu

China Agricultural University

Oleksandr Mialyk

University of Twente <https://orcid.org/0000-0002-7495-2325>

Sara Minoli

PIK

Elisabeth Moyer

University of Chicago <https://orcid.org/0000-0003-1829-5196>

Masashi Okada

National Institute for Environmental Studies

Meridel Phillips

Columbia University

Cheryl Porter

University of Florida <https://orcid.org/0000-0001-7269-6543>

Sam Rabin

Karlsruhe Institute of Technology

Clemens Scheer

Karlsruhe Institute of Technology

Julia Schneider

Ludwig-Maximilians-Universität München

Joep Schyns

University of Twente <https://orcid.org/0000-0001-5058-353X>

Rastislav Skalský

International Institute for Applied Systems Analysis <https://orcid.org/0000-0002-0983-6897>

Andrew Smerald

Karlsruhe Institute of Technology

Tommaso Stella

Leibniz Centre for Agricultural Landscape Research <https://orcid.org/0000-0002-3018-6585>

Haynes Stephens

University of Chicago <https://orcid.org/0000-0002-2258-5244>

Heidi Webber

Leibniz Centre for Agricultural Landscape Research <https://orcid.org/0000-0001-8301-5424>

Florian Zabel

Ludwig-Maximilians-Universität München <https://orcid.org/0000-0002-2923-4412>

Cynthia Rosenzweig

NASA Goddard Institute for Space Studies <https://orcid.org/0000-0002-8541-2201>

Article

Keywords: crop model, climate-related impacts, yield responses

Posted Date: August 12th, 2021

DOI: <https://doi.org/10.21203/rs.3.rs-101657/v1>

License:  This work is licensed under a Creative Commons Attribution 4.0 International License.

[Read Full License](#)

Version of Record: A version of this preprint was published at Nature Food on November 1st, 2021. See the published version at <https://doi.org/10.1038/s43016-021-00400-y>.

Climate change signal in global agriculture emerges earlier in new generation of climate and crop models

Jonas Jägermeyr^{1,2,3}, Christoph Müller³, Alex C. Ruane¹, Joshua Elliott⁴, Juraj Balkovic^{5,19}, Oscar Castillo⁶, Babacar Faye⁷, Ian Foster⁸, Christian Folberth⁵, James A. Franke^{9,4}, Kathrin Fuchs¹⁰, Jose Guarin^{1,2}, Jens Heinke³, Gerrit Hoogenboom^{6,11}, Toshichika Iizumi¹², Atul K. Jain¹³, David Kelly⁸, Nikolay Khabarov⁵, Stefan Lange³, Tzu-Shun Lin¹³, Wenfeng Liu¹⁴, Oleksandr Mialyk¹⁵, Sara Minoli³, Elisabeth J. Moyer^{9,4}, Masashi Okada¹⁶, Meridel Phillips^{1,2}, Cheryl Porter⁶, Sam Rabin¹⁰, Clemens Scheer¹⁰, Julia M. Schneider¹⁷, Joep F. Schyns¹⁵, Rastislav Skalsky^{5,20}, Andrew Smerald¹⁰, Tommaso Stella¹⁸, Haynes Stephens⁹, Heidi Webber¹⁸, Florian Zabel¹⁷, Cynthia Rosenzweig¹

¹NASA Goddard Institute for Space Studies, New York, USA

²Columbia University, Center for Climate Systems Research, New York, USA

³Potsdam Institute for Climate Impacts Research (PIK), Member of the Leibniz Association, Potsdam, Germany

⁴Center for Robust Decision-making on Climate and Energy Policy (RDCEP), University of Chicago, Chicago, USA

⁵International Institute for Applied Systems Analysis, Laxenburg, Austria

⁶Agricultural & Biological Engineering Department, University of Florida, Gainesville, Florida, USA

⁷Institut de recherche pour le développement (IRD) ESPACE-DEV, Montpellier, France

⁸Department of Computer Science, University of Chicago, Chicago, Illinois, USA

⁹Department of the Geophysical Sciences, University of Chicago, Chicago, Illinois, USA

¹⁰Institute of Meteorology and Climate Research, Atmospheric Environmental Research, Karlsruhe Institute of Technology, Garmisch-Partenkirchen, Germany

¹¹Institute for Sustainable Food Systems, University of Florida, Gainesville, Florida, USA

¹²Institute for Agro-Environmental Sciences, National Agriculture and Food Research Organization, Tsukuba, Japan

¹³Department of Atmospheric Sciences, University of Illinois, Urbana, Illinois, USA

¹⁴Center for Agricultural Water Research in China, College of Water Resources and Civil Engineering, China Agricultural University, Beijing, China

¹⁵Multidisciplinary Water Management group, University of Twente, Enschede, The Netherlands

¹⁶Center for Social and Environmental Systems Research, National Institute for Environmental Studies, Tsukuba, Japan

¹⁷Ludwig-Maximilians-Universität München (LMU), Munich, Germany

¹⁸Leibniz Centre for Agricultural Landscape Research (ZALF), Müncheberg, Germany

¹⁹Faculty of Natural Sciences, Comenius University in Bratislava, Bratislava, Slovak Republic

²⁰Soil Science and Conservation Research Institute, National Agricultural and Food Centre, Bratislava, Slovak Republic

Potential climate-related impacts on future crop yield are a major societal concern first surveyed in a harmonized multi-model effort in 2014. We report here on new 21st-century projections using ensembles of latest-generation crop and climate models. Results suggest markedly more pessimistic yield responses for maize, soybean, and rice compared to the original ensemble. Mean end-of-century maize productivity is shifted from +5 to -6% (SSP126) and +1 to -24% (SSP585) — explained by warmer climate projections and improved crop model sensitivities. In contrast, wheat shows stronger gains (+9 shifted to +18%, SSP585), linked to higher CO₂ concentrations and expanded

46 **high-latitude gains. The ‘emergence’ of climate impacts — when the change signal**
47 **emerges from the noise — consistently occurs earlier in the new projections for several**
48 **main producing regions before 2040. While future yield estimates remain uncertain, these**
49 **results suggest that major breadbasket regions will face distinct anthropogenic climatic**
50 **risks sooner than previously anticipated.**

51

52

53 Climate change already affects agricultural productivity worldwide via many mechanisms, driven
54 largely by warmer mean and extreme temperatures, altered precipitation regimes and drought
55 patterns, and elevated atmospheric CO₂ concentrations ([CO₂])¹. Uncertainties arising from
56 greenhouse gas emission scenarios, climate model projections, and the understanding and
57 representation of complex impact processes render estimates of future crop yield highly
58 uncertain². A way towards improving yield projections is the development of benchmarked multi-
59 model ensemble simulations driven by harmonized simulation protocols³. Facilitated by the
60 Agricultural Model Intercomparison and Improvement Project (AgMIP)⁴ and the Inter-Sectoral
61 Impact Model Intercomparison Project (ISIMIP)⁵, here we present a new systematic assessment
62 of agricultural yield projections, based on a protocol similar to the one used by Coupled Model
63 Intercomparison Project (CMIP) for climate models⁶. Previous projections of AgMIP’s Global
64 Gridded Crop Model Intercomparison (GGCMI) based on CMIP5 identified substantial climate
65 impacts on all major crops, with strong temperature and CO₂ responses and regional patterns of
66 losses and gains⁷. As the first systematic intercomparison, GGCMI-CMIP5 (hereafter ‘GC5’)
67 demonstrated in 2014 that crop models might indeed introduce larger uncertainty than current
68 climate models. CMIP6 now provides new reference climate model projections^{8,9}, and recently
69 improved bias-adjustment and downscaling methods¹⁰ benefit the impact modeling community
70 and support an advanced ensemble of process-based crop models. With improved and further
71 harmonized inputs and configuration of cropping systems, GGCMI is able to provide a new
72 standard in crop yield projections for the 21st century for several major crops using state-of-the-
73 art modeling approaches with CMIP6 scenarios (hereafter ‘GC6’).

74

75 Climate change impacts are often quantified in terms of differences over time, but especially in
76 view of adaptation measures, it is the amplitude of the change compared to the local
77 background variability and uncertainty of the recent past that is often more relevant¹¹. Time of
78 climate impact emergence (TCIE) — the point in time by which the yield levels of exceptional
79 years (negative or positive) have become the new norm — is a critical measure for risk
80 assessment. Time of emergence¹² metrics have been applied to climate variables including
81 temperature^{13,14}, precipitation¹⁵, and others^{16,17} and demonstrate that major food producing
82 regions are increasingly facing changing climate profiles in the near term. Here we introduce the
83 TCIE concept with respect to future agricultural risks.

84

85 The analyses presented here shed new light on the projected effects of elevated [CO₂], which
86 have been neglected in many previous studies that focused on direct temperature responses^{18–}
87 ²⁰. CO₂ effects are among the largest sources of uncertainty inflating the range of crop model
88 projections by the end of the century^{21–24}, but they must be reflected in plausible future yield
89 projections²⁵. The uncertainty in the mechanisms and overall size of the effects of CO₂
90 fertilization manifested in farmers' fields are reflected in a wide range of CO₂ sensitivities among
91 the crop models contributing to the GGCM archive^{21,25}.

92

93 Here we present an ensemble of process-based projections of global productivity estimates for
94 the major crops for the 21st century. This work represents the first update since GC5 in 2014⁷
95 and includes updated climate projections based on CMIP6 and latest-generation crop models
96 for maize, wheat, rice, and soybean. This study is based on constant management
97 assumptions, focusing on the isolated climate change effect on current crop production
98 systems. Opportunities associated with farming system adaptation and management trends will
99 be addressed in upcoming GGCM simulations.

100

101 The simulation protocol is based on two Shared Socioeconomic Pathways related to
102 Representative Concentration Pathways (RCPs), RCP2.6 and RCP8.5 (hereafter ‘SSP126’ and
103 ‘SSP585’; adaptation measures associated with the SSPs are not considered)⁹, chosen to
104 sample the range of available scenarios²⁶ and to make the results comparable with GC5.
105 Twelve GGCMs each simulated 5 GCM forcings, resulting in nearly 240 climate-crop model
106 realizations per crop (GGCMs x GCMs x RCPs x CO₂ settings). The climate projections from the
107 5 GCMs (Table S1), centrally bias-adjusted and downscaled for different research sectors, were
108 selected by ISIMIP based on benchmark performance, equilibrium climate sensitivity, and
109 output availability (see Methods). All simulations were carried out globally on a 0.5° grid,
110 covering the time period 1850 to 2100. We evaluate results based on the transient atmospheric
111 CO₂ concentration (i.e., ‘default’ [CO₂]) and only refer to counterfactual simulations without
112 [CO₂] increase after the year 2015 (‘constant’ [CO₂]) to quantify the CO₂ fertilization effect for
113 further uncertainty evaluation and climate change factor attribution.

114

115 Recent literature has focused on capturing the temperature sensitivity of crops^{18–20,27–29} in
116 isolation. To quantify climate change impacts more comprehensively, additional factors
117 including precipitation changes, temperature-moisture feedbacks, and [CO₂] need to be
118 considered. The aims of this first GC6 study are to: i) provide new ensemble projections for the
119 productivity of major crops under climate change, ii) assess climate change impacts on crop
120 yields from a risk perspective, employing the TCIE concept, iii) improve understanding of
121 regional patterns of change, and iv) explore drivers of uncertainty related to climate models,
122 crop models, and responses to [CO₂].

123 Global production response of major crops

124 The ensemble response across the new generation of climate and crop models to the SSP126
125 and SSP585 forcing is markedly more pronounced than in GC5⁷ (Fig. 1). Wheat results are

126 more optimistic, while maize, soybean, and rice results are decisively more pessimistic. For
127 maize, the most important global crop in terms of total production and food security in many
128 regions, the mean end-of-century (2069-2099) global productivity response is ~10% (SSP126)
129 and ~20% (SSP585) lower than in GC5. This shifts the SSP585 estimate from +1%
130 (interquartile range of crop-climate model combinations: -10 to +8%) to -24% (-38 to -7%) and
131 for SSP126 from +5 to -6%. For wheat, the second largest global crop in terms of production,
132 the SSP585 ensemble estimate is shifted upwards from +10% (-1 to +15%) to +18% (-2 to
133 +39%), and under SSP126 from +5 to +9%. The SSP585 ensemble estimates for soybean are
134 revised downward from +15% (-8 to +36%) to -2% (-21 to +17%) and for rice from +23% (+1 to
135 +33%) to +2% (-15 to +12%). Overall, the new climate and crop model combinations narrow the
136 range of crop yield projections for soybean and rice, but disagreement among crop models
137 remains substantial and is largely indecisive about the sign of change at the global level (p-
138 value > 0.5 for both crops). The maize and wheat responses are robust and became more
139 distinct since GC5. While the range of crop projections somewhat increased, 85% of model
140 combinations indicate negative maize changes and 73% project positive wheat changes under
141 SSP585. Both responses are now statistically significant (p-value < 10⁻⁵); the maize response in
142 GC5 was not (p-value > 0.6). There is larger agreement on positive change for wheat under
143 SSP126 (89%) than under SSP585, indicating peak-and-decline trajectories for parts of the
144 ensemble under high-emissions scenarios (Fig. S1).

145

146 As a C₄ crop, maize has a smaller capacity to benefit from elevated [CO₂]³⁰, and it is also grown
147 across a wider range of low latitudes that are projected to experience the largest adverse
148 impacts due in large part to current proximity to crop-limiting temperature thresholds³¹. As a C₃
149 crop, the positive wheat response is explained by its relatively stronger CO₂ response and the
150 fact that global warming leads to wheat yield increases in high-latitude regions that are currently
151 temperature-limited²⁹.

152

153 Three factors explain the more-pronounced crop yield response in GC6. First, CMIP6 has
154 markedly higher [CO₂] than CMIP5 (Fig. 2), with year 2099 concentrations increased from 927
155 ppm (RCP8.5) to 1122 ppm (SSP585)⁹. Second, CMIP6 has a higher average end-of-century
156 warming level compared to CMIP5, adequately represented in the 5 GCMs sampled here (Table
157 S1, S2). While both RCP2.6 and RCP8.5 are on average ~0.3 °C warmer in CMIP6 than CMIP5
158 over land and oceans, the difference is even more pronounced (>0.5 °C) across main maize-
159 producing regions (Fig. 2). Third, the new crop model ensemble features advanced versions of
160 previous models, several new members, and improved input data, which resulted in more
161 realistic sensitivities to climate and [CO₂] changes (see details below).

162 Emergence of the climate change signal in agriculture

163 The Time of Climate Impact Emergence (TCIE) describes the point in time when average
164 climate change impacts are projected to occur outside the envelope of historical variability and
165 uncertainty ('noise'). We define TCIE as the year in which the multi-model 25yr moving-average
166 crop production change ('signal') emerges from the noise (i.e., standard deviation of simulated
167 variability across all GCM x GGCM combinations in 1983-2013).

168

169 Maize consistently shows emerging negative productivity changes ('negative TCIE') among
170 major producer regions. The ensemble median signal emerges from the noise at global level in
171 the year 2032 under SSP585 and the year 2051 under SSP126 (Fig. 3). Of all individual GCM x
172 GGCM realizations, 84% show a negative TCIE by 2099 under SSP585 (52% under SSP126)
173 and the inter-quartile range spans from 2014 to 2056, indicating sizeable agreement among
174 models. This is a substantial shift away from the GC5 simulations in which the ensemble
175 median shows no emergence by 2099 under any emission pathway, only seen in 46% of
176 individual GCM x GGCM combinations under RCP8.5 (inter-quartile range 2044-2080). Overall,

177 the TCIE signal at global level is shifted 30-40 years earlier and is more pronounced in the new
178 generation of climate and crop model projections (Fig. 4).

179

180 By the end of the century, 10% (SSP126) to 74% (SSP585) of current global maize cultivation
181 areas are projected to undergo negative TCIE (Fig. 5). Under SSP585 this trajectory is markedly
182 earlier, with higher late-century fractions of cropland area affected compared to the respective
183 47% in GC5 (RCP8.5). Crop models indicate early negative maize TCIE before 2040 even
184 under SSP126 in Central Asia, the Middle East, Southern Europe, Western USA, and tropical
185 South America. Projections referencing the 1983-2013 period suggest that the mean yield signal
186 is already starting to emerge in some of these regions (Fig. 3e and Fig. 5), patterns largely in
187 line with recent observations^{15,32,33}. The tropical zone is the only climate zone in which the GC5
188 ensemble median also indicated a negative maize TCIE (Fig. 3e).

189

190 The standard deviation of grid-level TCIE estimates under SSP585 ranges between 25 and 35
191 years across most breadbasket regions, with slightly higher values under SSP126 (Fig. S2).
192 Such uncertainty ranges are in line with time of emergence estimates for climatological
193 variables, yet somewhat higher due to the additional layer of crop model uncertainties^{12,13}.
194 Clearest emergence signals, i.e., largest signal-to-noise ratios with values < -2 , are found
195 among lower latitudes in the tropics but also in Central Asia, the Middle East, and Western USA
196 (Fig. S3). As internal variability — and thus total noise — decreases with averaging, earlier
197 TCIE is generally found for larger spatial scales.

198

199 For wheat, ensemble projections indicate TCIE of positive productivity changes ('positive TCIE')
200 at the global level (Fig. 3b) and across large parts of currently cultivated areas (Fig. 5). While
201 also found in GC5 simulations, TCIE is shifted ~10 years earlier in GC6, suggesting that
202 climate-related increases might occur globally within the next few years (year 2023 under

203 SSP585, year 2025 under SSP126; inter-quartile ranges 2014-2029 and 2015-2029) and across
204 major breadbasket regions within the next two decades (Fig. 5). In some regions we already
205 detect a TCIE signal today, which is in line with the range of time of emergence estimates for
206 temperature and precipitation^{13,15}. Such effects are difficult to distinguish from rapidly changing
207 management practices in observational data, but climate change impacts have been
208 documented for example in Central and South Asia, Northern China, and the USA^{32,34}. The
209 TCIE estimates for wheat show high consistencies across the model ensemble — 76%
210 (SSP126) and 88% (SSP585) of individual model combinations show positive TCIE by 2099. As
211 for maize, the TCIE signal is shifted earlier and is more pronounced in GC6 than in GC5 (Fig.
212 4).

213

214 The share of wheat cultivation areas projected to see positive TCIE increased substantially in
215 GC6, from 8% (GC5, RCP8.5) to 37% (GC6, SSP585; Fig. 5f). This share levels off by mid-
216 century, a result of peak-and-decline trajectories seen in some crop models (Fig. 5f ; compare
217 Fig. 3d and Fig. S3 for regions that show TCIE early on but not by late century). Wheat also
218 exhibits negative TCIE among important growing regions in South Asia, Southern USA, Mexico,
219 and parts of South America around mid-century. The uncertainty among grid-level TCIE
220 estimates is generally higher for wheat than for maize (Fig. S2) and the extent of areas with very
221 high signal-to-noise ratios (i.e., >2) is smaller (Fig. S3).

222

223 Ensemble median soybean and rice productivity peak mid-century and decline towards the end
224 of the century at the global level (Fig. S4). The soybean response exhibits late-century negative
225 TCIE (year 2096) under SSP585; rice on the other hand shows early positive TCIE (year 2030,
226 SSP585) but late-century declines are not projected to reach the level of negative TCIE at the
227 global level. Rice is the only crop in this study that indicates positive TCIE in the tropics, which

228 drives early net global gains before productivity is simulated to decline again by about 2060
229 (Fig. S4c).

230 Regional patterns of yield change

231 Projections of crop yield changes include regions of losses and gains for all crops (Fig. 3, S4).
232 Global average responses can hide important regional changes, which are supported by strong
233 crop model agreement. Maize projections show spatially homogeneous losses especially
234 among main growing regions in North America, Mexico, West Africa, Central Asia, and China,
235 where crop model agreement is high (Fig. 3c). The high-latitude gains found in GC5 are not as
236 prevalent in GC6 and associated with high crop model uncertainty and low baseline yields.
237 Wheat shows distinct geographic gradients with losses in spring wheat regions in Mexico,
238 Southern USA, South America, and South Asia, supported by good model agreement. Sizable
239 wheat gains are projected by many models for the North China Plains, Australia, Central Asia,
240 Middle East, and for the winter wheat growing regions in the Northern USA and Canada (Fig.
241 3d). Soybean shows the greatest losses in the main-producer regions — the USA, Brazil, and
242 Southeast Asia — paired with large gains across parts of China and generally higher latitudes
243 (Fig. S4). Major declines in rice yields are simulated in Central Asia, and gains in South Asia,
244 NE China, and South America. Both soybean and rice yield changes must be interpreted in view
245 of the wide range in crop model ensemble results (Fig. 1, S4). A breakdown of yield responses
246 for the top-10 producer countries per crop highlights a wide range of CO₂ effects embedded in
247 the signal (Fig. S5, S6).

248

249 A latitudinal profile of yield changes under SSP585 — simulated in all grid cells irrespective of
250 the current cropland distribution — indicates that losses are most prevalent among low-latitude
251 tropical regions with highest gains found at higher latitudes beyond 50°N and 30°S for all crops
252 (Fig. 6). Maize exhibits widespread losses between 50°N and 30°S, while losses for the other

253 crops are more concentrated in the tropics with a less distinct signal for soybean and rice. Major
254 wheat breadbaskets are generally located at higher latitudes than maize, which further
255 contributes to overall wheat gains when aggregated across currently cultivated areas. Although
256 more than 90% of maize and wheat is currently produced in the temperate and subtropical
257 climate zones, major yield losses will affect the livelihoods and food security of many
258 smallholder farmers in the tropics. Overall, our results show that lower latitudes face the largest
259 losses for all crops, while higher latitudes see potential gains. These conclusions are in line with
260 the IPCC AR5³⁵ and recent studies^{7,36,37} and such uneven distribution of impacts may further
261 increase regional disparities that are a 'Reason for Concern'³⁸ regarding climate change risks.

262 Drivers of more pronounced ensemble response

263 It is difficult to determine to what degree the differences in crop yield projections between GC6
264 and GC5 can be explained by the new atmospheric forcing, the new crop model ensemble, or
265 new input data. A subset of GC6 and GC5 crop models that participated in both ensembles
266 (albeit in different versions) shows very similar responses compared with the respective full
267 ensemble, suggesting that the crop model selection does not explain the differences (Fig. 7).
268 Further, standardized comparisons of crop model responses to specific mean temperature
269 increases over cropland areas ('warming sensitivity'; under constant [CO₂] conditions, but
270 including changes in other climate variables) from 1-2°C and from 2-3°C, respectively, highlights
271 that the isolated warming sensitivity in GC6 has substantially increased for maize (from 2-3% in
272 GC5 to 8-9% in GC6) and decreased for wheat (from 7% to 3-6%; Fig. 7). With higher overall
273 warming levels in CMIP6, net warming-related maize losses by 2069-2099 thus increased from
274 12% (4.6°C maize cropland warming) to 30% (5°C maize cropland warming) in GC6. Further,
275 the CO₂ sensitivity at 500 and 700 ppm, but also net effects by the end of the century, have
276 decreased for both maize and wheat. In summary, the more pessimistic maize response in GC6
277 can largely be attributed to a higher sensitivity to warming and a lower compensating effect due

278 to CO₂ fertilization in the crop models, and to a smaller extent to the higher absolute warming
279 levels in CMIP6. For wheat on the other hand, the more optimistic response in GC6 can be
280 explained by lower losses per degree warming (with stronger temperature-related gains in high-
281 latitude regions), overcompensating for a lower CO₂ fertilization effect than in GC5 (despite
282 higher total [CO₂] levels). For soybean and rice, in contrast, the more pessimistic response in
283 GC6 is largely attributed to higher warming levels in CMIP6 compounded by a higher crop
284 model sensitivity to warming, with similar sensitivities to changes in [CO₂] (Fig. S7).

285 Crop and climate model uncertainty

286 The range of crop model responses under SSP585 (mean across climate models) is
287 substantially larger than the range introduced by the five climate models (mean across crop
288 models; Fig. 1). However, for all crops and RCPs, the uncertainty associated with the five
289 CMIP6 climate models has increased compared to the five climate models sampled in GC5. In
290 turn, the fraction of total variance induced by the crop models is substantially reduced for all
291 crops in GC6 (for maize from 97 to 69%; Fig. 8), which highlights that the crop response
292 became more consistent, even though the number of crop models increased. Absolute variance
293 induced by the climate models has increased for all crops (Fig. 8),
294 which is explained by a wider distribution of climate sensitivities tracked by the five CMIP6
295 GCMs (Table S1, S2), but also by higher [CO₂] assumed in CMIP6 (Fig. 2). In this sample,
296 UKESM1 is the most pessimistic GCM for both RCPs and all crops, the global mean warming
297 level by 2099 is about 2.6°C higher than in GFDL-ESM4, and the Transient Climate Response
298 is 1.2°C higher (see Table S1 for more details)⁶. Generally, the least pessimistic crop impacts
299 are found with MRI-ESM2 (Fig. 1).

300

301 Higher emission scenarios inflate the crop model uncertainty (SSP585), while the overall
302 climate- and crop model-induced uncertainty range in GC6 is of comparable size under SSP126

303 (Fig. 1). Uncertainty in the CO₂ effect causes much of the crop model uncertainty for wheat,
304 soybean, and rice (Fig. S8), yet the range of maize responses is not fundamentally reduced
305 without the CO₂ effect. In line with physiological knowledge³⁰, crop models mostly show the
306 smallest CO₂ effects for C₄ crops (maize) and much larger responses for C₃ crops (wheat,
307 soybean, rice). However, the CO₂ effects differ widely across crop models; the ensemble
308 median rainfed response is 19% for maize, 33% for wheat, 48% for soybean, and 37% for rice
309 by the year 2099 (Fig. S8), which is generally in line with field experiments given that model
310 simulations include nutrient limitations^{25,30}. CYGMA and CROVER exhibit a strong peak-and-
311 decline CO₂ response for some crops, resulting in negative CO₂ effects for maize in CYGMA
312 after 2090 (Fig. S8). This is driven by increased water use efficiencies under elevated [CO₂],
313 eventually leading to adverse excess moisture effects in humid regions — a new feedback
314 represented primarily in CYGMA and underexplored in previous studies³⁹.

315

316 In addition to the CO₂ effect, climate change affects simulations of crop growth and
317 development in various ways. These include for example changed precipitation patterns,
318 extreme heat and drought events, and importantly, accelerated maturity. Higher temperatures
319 lead to faster phenological development and substantial reductions in the growing season
320 length in all crop models (Fig. S9), which in turn lead to complex processes affecting yield,
321 including shorter grain filling periods, smaller canopy, and reduction in photosynthesis. This
322 effect varies across models and additional work is needed to further narrow the range of crop
323 model responses⁴⁰. After all, the standard deviation of simulated yield variability matches
324 observational data to a much higher degree in GC6 (R = 79%) than in GC5 (R = 44%), adding
325 to more realistic yield responses (Fig. S10).

326 Discussion

327 We introduce the concept of climate impact emergence to the field of agriculture impacts,
328 highlighting that major shifts in global crop productivity due to climate change are projected to
329 occur within the next twenty years, several decades sooner than estimates based on previous
330 model projections. The impact on crop productivity under SSP126 and SSP585 is largely similar
331 for the coming decade, which leaves little room for climate mitigation efforts. In light of the much
332 larger climate and crop model agreement for these short-term projections than for the late
333 century, the findings highlight challenges for food system adaptation faced with significantly
334 shorter lead times.

335

336 These CMIP6 multi-model crop yield projections suggest that climate change impacts on global
337 agriculture will be more pronounced than in GC5, with substantially larger losses for maize,
338 soybean, and rice and additional gains for wheat. This is supported by a generally more
339 consistent crop model ensemble. However, large uncertainties remain, particularly in TCIE
340 estimates — the standard deviation for global maize TCIE is 24 years (SSP585), which is
341 similar to estimates of temperature emergence¹². Yet the signal is robust: More than 80% of the
342 GCM-GGCM combinations indicate TCIE for maize and wheat by late century across major
343 breadbaskets (SSP585). TCIE estimates based on different metrics qualitatively agree (e.g.,
344 multi-model ensemble mean TCIE for maize is found in the year 2032, the median of individual
345 GCM x GGCM estimates in the year 2027, and the mean in the year 2036). Leaving one crop
346 model out at a time introduces a TCIE standard deviation of only 1.5 years for both maize and
347 wheat (SSP585). That said, time of emergence estimates are sensitive to the underlying
348 definitions (e.g., noise, pre-industrial or recent climate, smoothing approach, threshold
349 selection) and can push the emergence date earlier or later in time^{12,13,15,41}. Absolute TCIE

350 estimates are therefore more challenging to interpret than relative comparisons among regions,
351 crops, and especially the two ensemble projections GC5 and GC6.

352

353 Wheat yield increases are projected to level off by midcentury and part of the climate-crop
354 model ensemble indicates net losses under SSP585 by 2099 (Fig. 1, S1). Maize yield on the
355 other hand is projected to decline steadily, supported by higher model agreement than for
356 wheat. These general response differences are also in line with previous findings⁴². The more
357 pronounced response of the new projections can be explained primarily by higher equilibrium
358 climate sensitivities, higher [CO₂], and different crop model sensitivities per degree warming and
359 [CO₂] changes. With regard to CMIP6, higher and wider-ranging climate sensitivities are
360 critically discussed and associated with differing parameterizations of cloud feedback and cloud-
361 aerosol interactions^{14,43–49}. While better simulations of cloud liquid water contents and their
362 radiative behavior render the climate models more realistic, it is unclear whether these
363 improvements translate into more accurate estimates of equilibrium climate sensitivity (ECS)
364 and overall warming levels. Additional improvements of the GCMs, and the bias-adjustment and
365 downscaling methods used, result in better representations of extreme events and internal
366 variability^{10,47,50–52}, which are critical for crop modeling. Higher [CO₂] in CMIP6 are due to a
367 revised tradeoff between [CO₂] and [CH₄] resulting from updated observations and assumptions
368 in the MAGICC7.0 model⁵³.

369

370 The GGCM crop model ensemble has substantially changed and consists of revised and new
371 members. For example, LPJmL contributed to GC5 and has since been fundamentally improved
372 with the addition of the nitrogen cycle⁵⁴ and heat unit parameterization⁵⁵. In addition, input data
373 and model harmonization have been improved, including growing season harmonization based
374 on a new crop calendar developed for this study (see Methods). A comprehensive attribution of
375 crop response differences between GC5 and GC6 to changes in climate forcing, crop model

376 selection and sensitivities, and input data is not feasible. But standardized comparisons of
377 changes in cropland warming and [CO₂] indicate that for maize and wheat changes in crop
378 model ensemble sensitivities dominate the response, and for soybean and rice higher warming
379 levels and warming sensitivity explain much of the differences (Fig. 7, S7).

380

381 The new GCM bias adjustment, crop model advancement, improved input data, and a new crop
382 yield bias correction serve to substantially reduce the amount of variance induced by the crop
383 models compared to the climate models, rendering the new GC6 ensemble more balanced and
384 consistent than GC5 despite a larger ensemble size (12 crop models in GC6, 7 in GC5; Fig. 8).

385 In a similar vein, Müller et al.⁵⁶ comprehensively compared crop yield uncertainties under all
386 CMIP5 and CMIP6 GCMs based on GGCM crop model emulators⁵⁷, confirming that CMIP6
387 introduces a wider range of yield responses with more pessimistic average impacts. In view of
388 improved model harmonization, inputs, and GGCM versions and performance, we consider
389 GC6 more reliable than GC5 – despite ongoing discussions on the temperature sensitivity in
390 CMIP6.

391

392 The wide range of CO₂ effects across GGCM models is generally in line with field
393 experiments^{25,58,59}, but the broad range of simulated CO₂ fertilization effects merits more
394 rigorous model testing at the process level, which in turn requires better reference data,
395 especially at high [CO₂] levels. Moreover, elevated [CO₂] boosts crop yield, but it may also affect
396 the nutritional content of the crops^{60–62}. Impacts related to excess moisture, water resource
397 limitations, and new distributions of pests and diseases may lead to additional regional biotic
398 stresses requiring follow-on analysis.

399

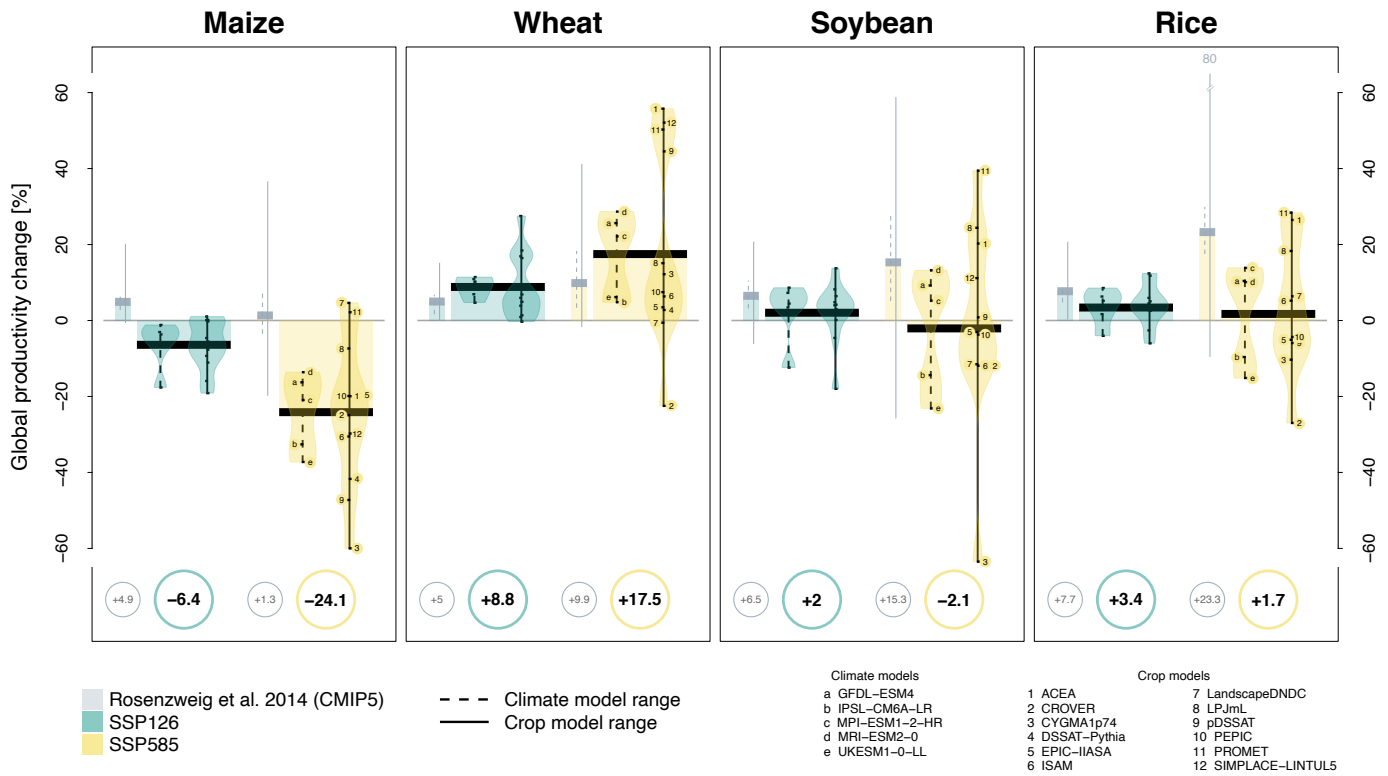
400 Cropping system adaptation can substantially reduce and even outweigh adverse climate
401 change impacts, for example by switching to other crops⁶³ or better-adapted varieties^{27,64}.

402 Integrated into ISIMIP's wider cross-sector activities, GGCM will systematically evaluate
403 farming system adaptation and changes in yield variability and extreme event impacts in
404 subsequent efforts.

405

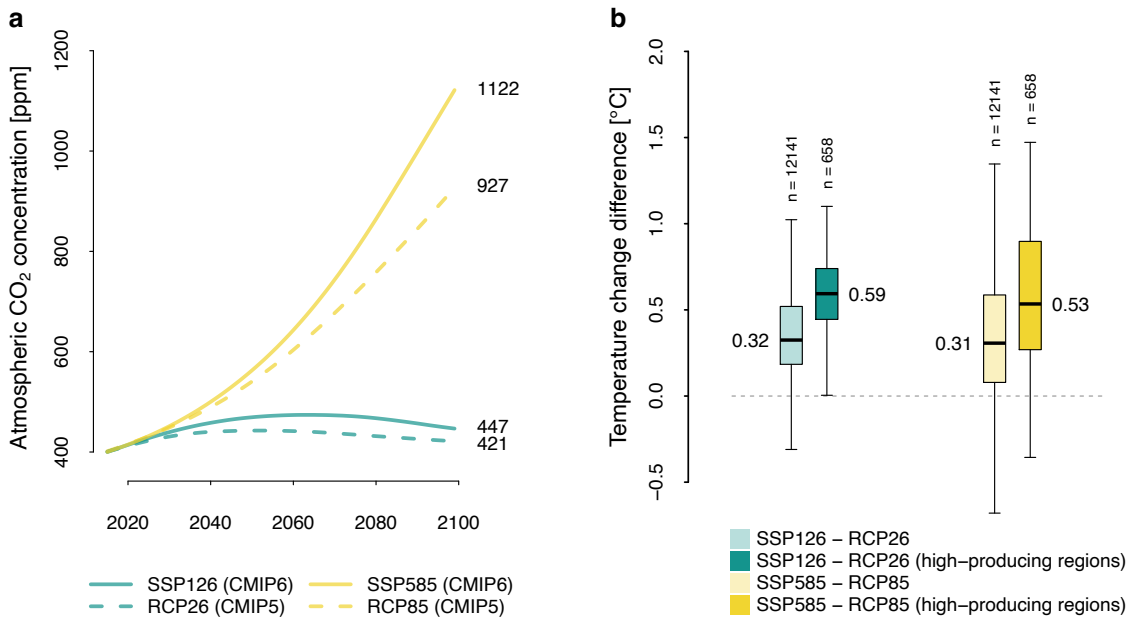
406 In conclusion, the new generation of AgMIP's GGCM provides the most comprehensive
407 ensemble of process-based future crop yield projections under climate change to date. The
408 degree to which even high mitigation climate change scenarios are projected to push global
409 farming outside of its historical regimes suggests that current food production systems will soon
410 face fundamentally changed risk profiles. Despite prevailing uncertainties, these ensemble
411 projections spotlight the need for targeted food system adaptation and risk management across
412 the main producer regions in the coming decades.

413



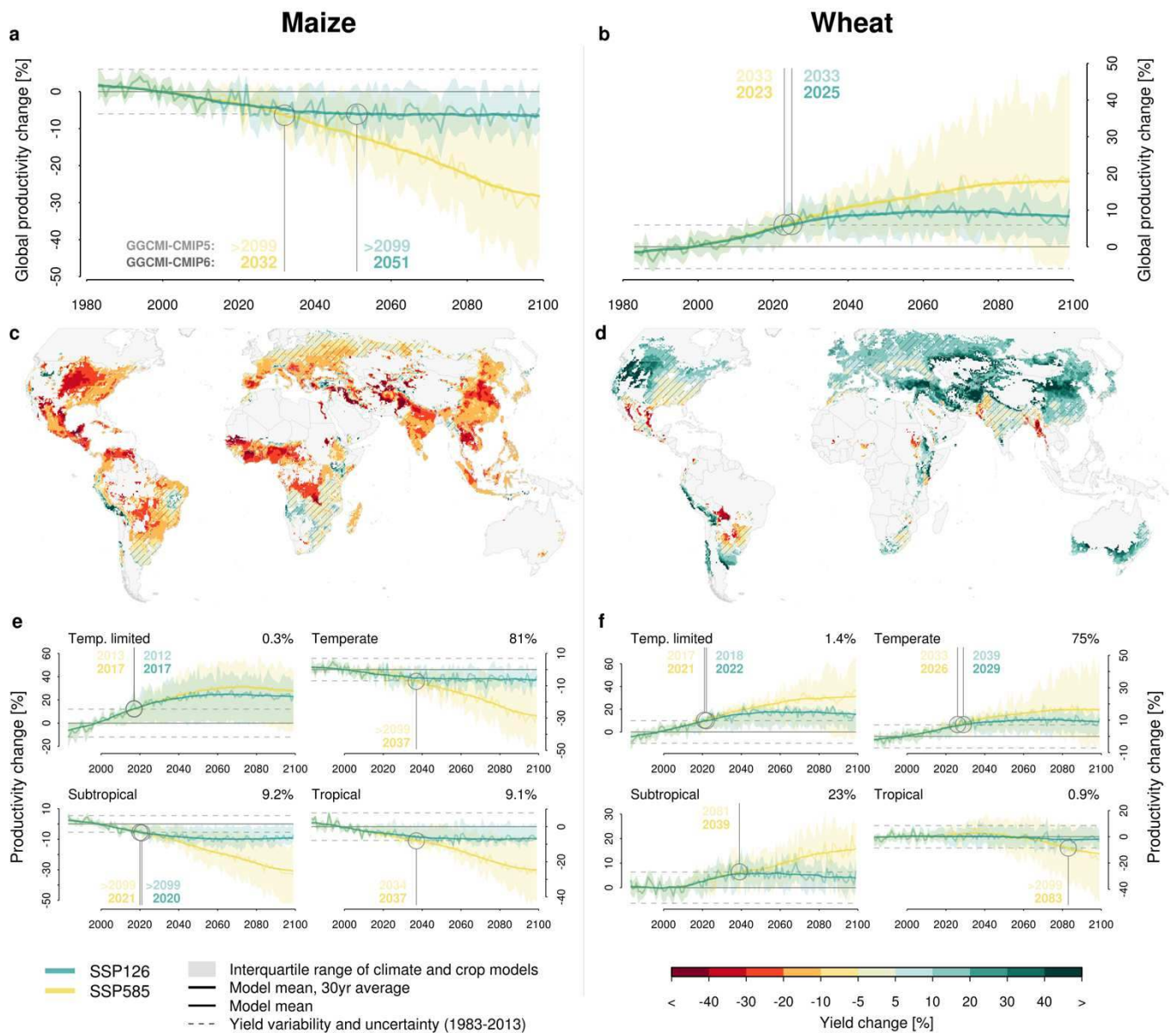
415

416 **Fig. 1: Ensemble end-of-century crop productivity response.** Global productivity changes (2069-2099
 417 compared to 1983-2013) for SSP126 and SSP585 are shown as the mean across climate and crop models
 418 for the four major crops (highlighted by bullets underneath the plot). Whiskers indicate the range of individual
 419 climate model realizations (dashed line, as the mean across crop models), and the range across crop
 420 models (solid line, as the mean across climate models). Individual model results are indicated by the bullets
 421 along the whisker lines (for SSP585 only); violin shades additionally highlight the model distribution. For
 422 context, gray bars and whiskers reference previous GGCM simulations based on CMIP5 (GC5; Rosenzweig
 423 et al. 2014)⁷ in the same way, without specifying individual models. Data are shown for the default [CO₂].
 424 Not all crop models simulate all crops, see Table S3 for details.
 425



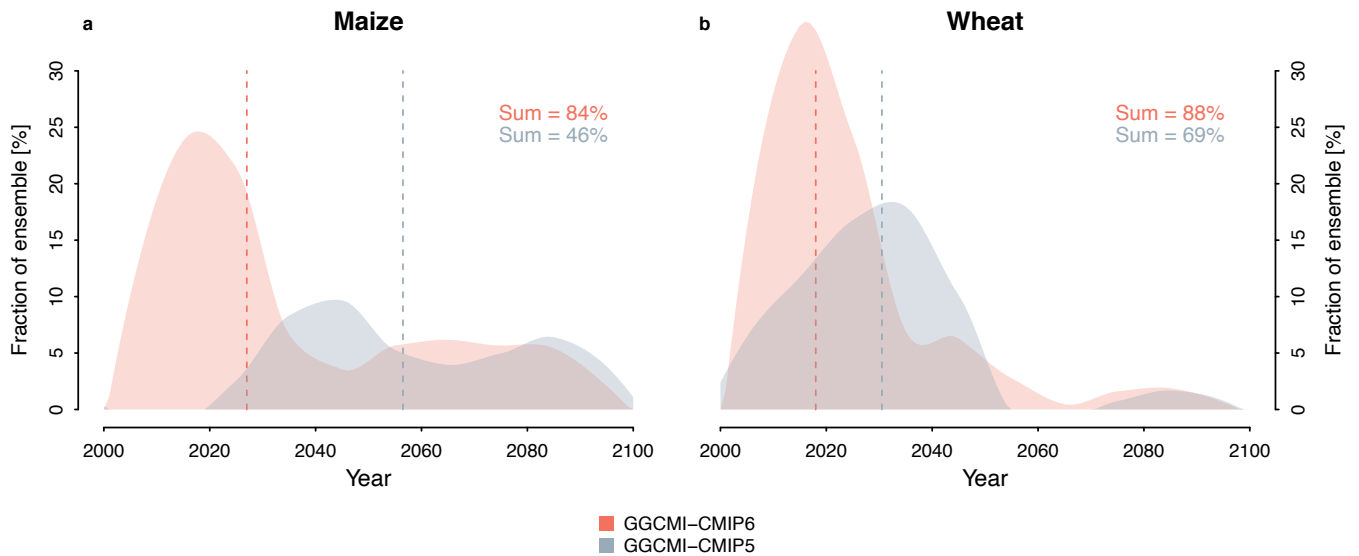
426

427 **Fig. 2: Comparison of [CO₂] and temperature changes between CMIP5 and CMIP6.** [CO₂] pathways for
 428 RCP26 and RCP85 in CMIP5 compared to SSP126 and SSP585 in CMIP6 (a). Box-and-whisker plots (b)
 429 show the difference of the average maize growing season temperature changes [°C] (2069-2099 compared
 430 to 1983-2013) between the CMIP6 and CMIP5 ensemble. Each ensemble is represented by the mean of 5
 431 GCMs (Table S1 and S2) in each grid cell. CMIP6 and CMIP5 differences are separated for SSP126 (green)
 432 and SSP585 (yellow) for all grid cells (maize production > 0; lighter shade) and for the highest-producing
 433 grid cells that together account for 50% of global production (darker shade).



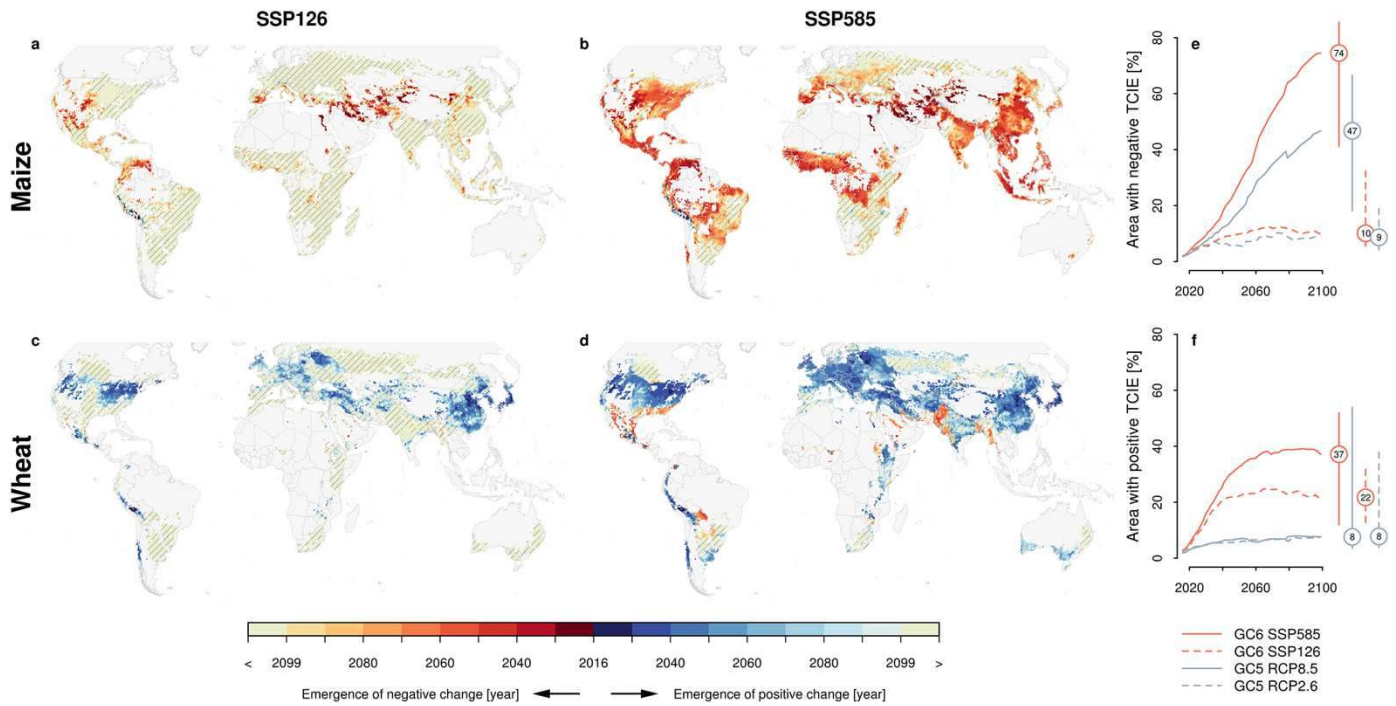
434

435 **Fig. 3: Projections of global crop productivity for the 21st century.** For maize (a) and wheat (b),
 436 productivity time series are shown as relative changes to the 1983-2013 reference period under SSP126
 437 (green) and SSP585 (yellow). Shaded ranges illustrate the interquartile range of all climate-crop model
 438 combinations (5 GCMs x 12 GGCMs). The solid line shows the median response (and a 25yr moving
 439 average). Horizontal dashed lines mark the standard deviation of historical yield variability and model
 440 uncertainty (i.e., 'noise' from individual climate-crop model combinations) and open circles highlight the
 441 'Time of Climate Impact Emergence' (TCIE), the year in which the smoothed climate change response
 442 emerges from the noise. For context, the TCIE calculated from GC5⁷ simulations is indicated in lighter
 443 shades above the TCIE based on GC6 (>2099 if no TCIE occurs by 2099). The maps (c, d) show median
 444 yield changes (2069-2099) under SSP585 across climate and crop models for current growing regions (>10
 445 ha). Hatching indicates areas where less than 70% of the climate-crop model combinations agree on the
 446 sign of impact. Regional productivity time series (e, f) are similar to (a), but stratified for the four major
 447 Koeppen-Geiger climate zones (temperature limited, temperate/humid, subtropical, and tropical). The
 448 percentage of the total global production contributed by each zone is indicated in the top right corner of the
 449 insets. All data are shown for the default [CO₂] (see Fig. S4 for all four crops).



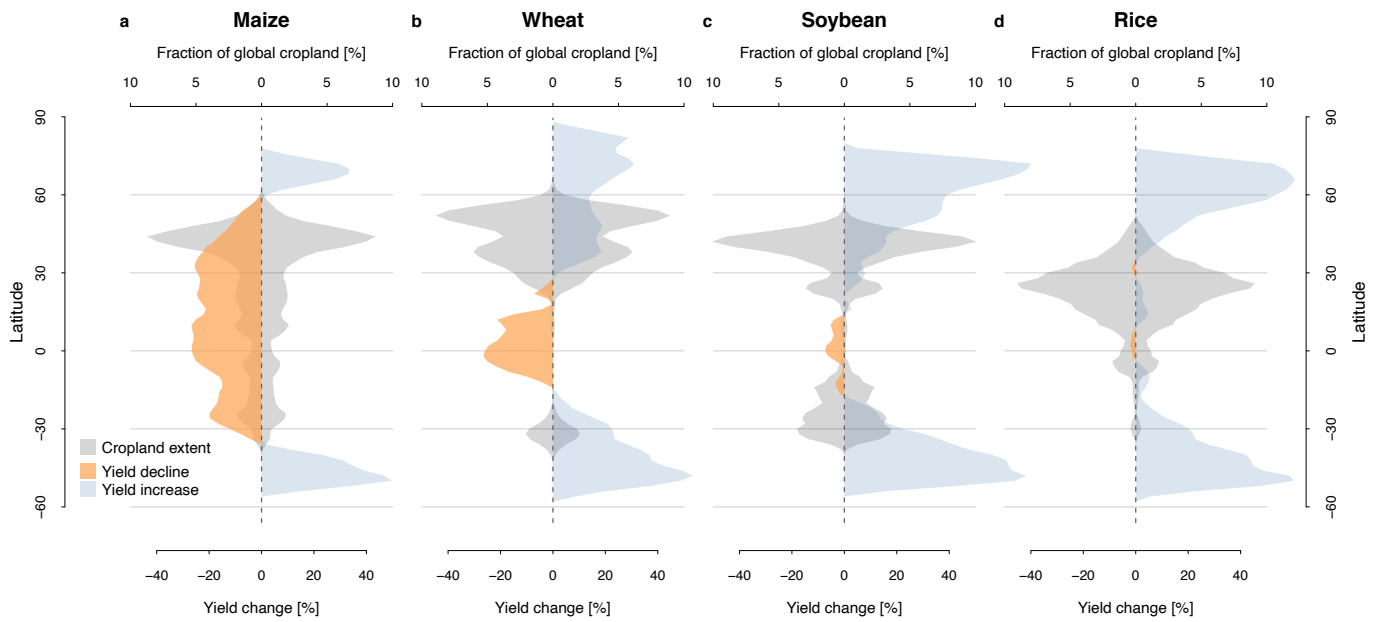
450

451 **Fig. 4: Shift towards earlier and more pronounced climate impact emergence.** Density plots of
 452 individual TCIE estimates across the GCM x GGCM ensemble under SSP585 are shown for global maize
 453 productivity (a; negative TCIE) and wheat (b; positive TCIE). Histogram counts are smoothed with a loess fit
 454 (span=0.5) and shown as the fraction of the respective ensemble size. The GGCM-CMIP6 ensemble
 455 includes 12 crop models, GGCM-CMIP5 includes 7 crop models; both comprise 5 GCMs. The total
 456 ensemble fraction that shows TCIE by 2099 is indicated in the top-right corner ('Sum'). The ensemble
 457 median TCIE is highlighted with vertical dashed lines.



458
 459
 460
 461
 462
 463
 464
 465
 466
 467
 468
 469
 470

Fig. 5: Geographic patterns in TCIE. The maps show TCIE estimates for maize (a, b) and wheat (c, d) under SSP126 and SSP585 — calculated as the median of individual TCIE estimates from each climate-crop model combination. Hatching indicates areas in which less than 70% of the crop models agree on the emergence signal by 2099. See Figure S2 for the associated standard deviation of TCIE estimates, and Figure S3 for the signal-to-noise ratio. Panel (e) and (f) illustrate the annual percentage of the respective global cropland area affected by negative (maize) and positive (wheat) TCIE under SSP126 and SSP585, separated for results from GC5⁷ and GC6. Vertical bars indicate the inter-quartile range of all climate-crop model combinations, with the median value in the circle. The maps show the first TCIE occurrence, even if the signal is reversed by late century (e.g., parts of India for wheat; compare with Fig. S3); estimates of the affected areas (e, f) account for signal changes.



471

472

473

474

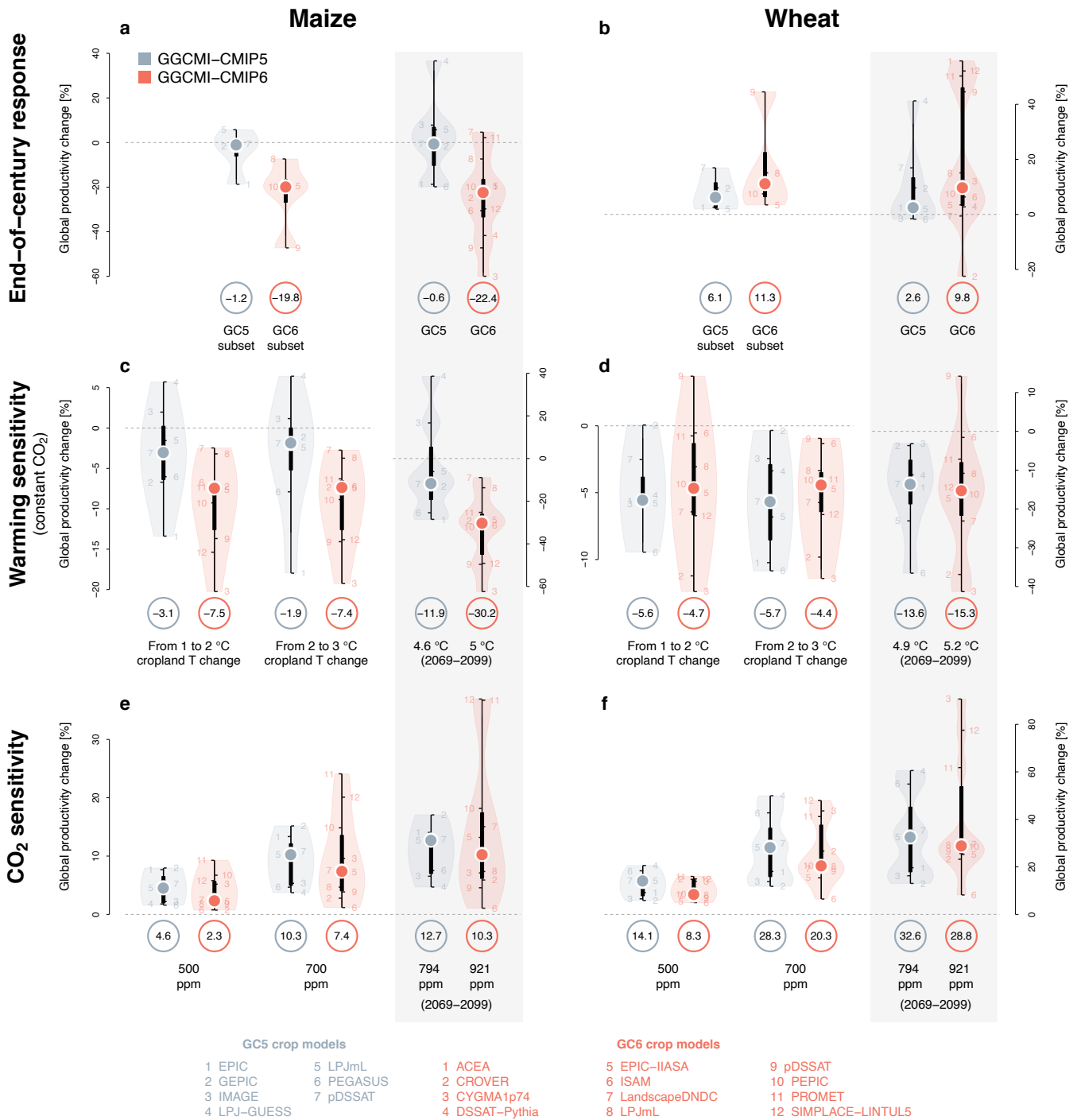
475

476

477

478

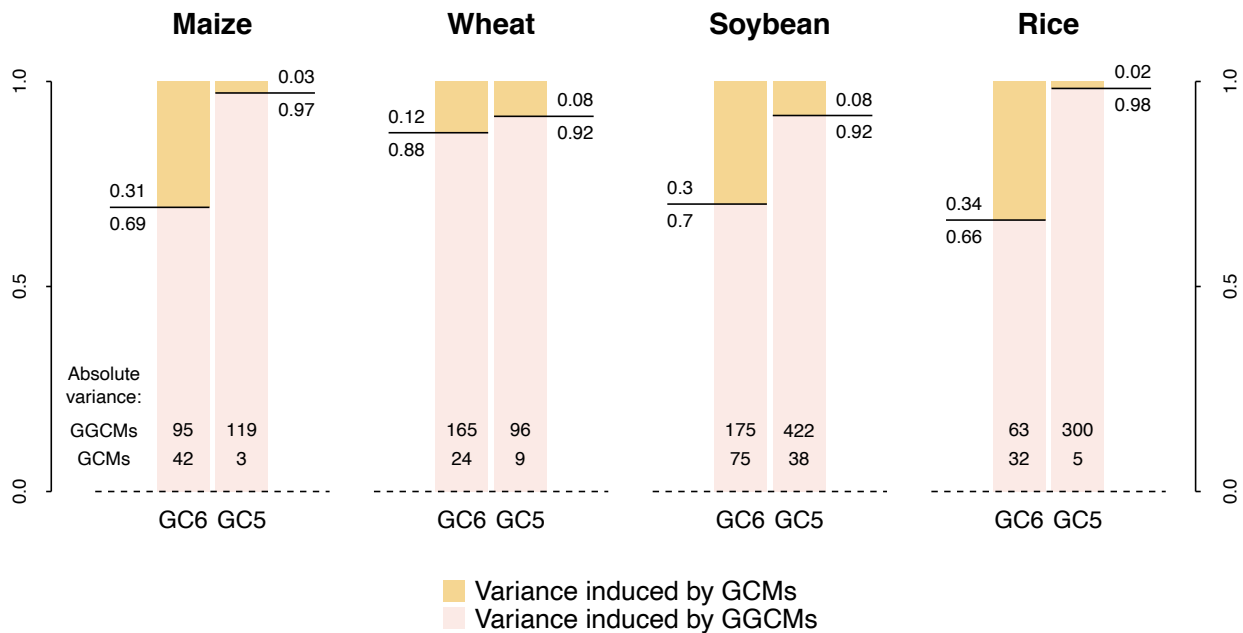
Fig. 6: Latitudinal profile of crop yield changes. Yield changes (SSP585, 2069-2099) are shown as latitude averages for maize (a), wheat (b), soybean (c), and rice (d), based on crop simulations in all grid cells, unconstrained by current cropland extent (bottom x-axis). For context, the current cropland extent is shown across latitude bands as fractions of the crop-specific global extent (top x-axis; mirrored to allow overlaps with both positive and negative yield changes). Yield data are shown as the climate and crop model median (marginal areas with yield lower than the 20th percentile per crop are excluded).



479

480 **Fig. 7: Driver attribution of crop model responses.** Projected end-of-century global productivity changes
 481 for maize (a) and wheat (b) under RCP8.5 (climate model mean) are shown for all members of the crop
 482 model ensemble GGCM-IP5 (GC5) and GGCM-IP6 (GC6), and for a subset of crop models that
 483 participated in both rounds (note substantial differences between model versions). The sensitivity to global
 484 mean warming (c, d) of the full ensembles is shown for temperature changes (over respective cropland
 485 areas per crop) from 1 to 2°C, from 2 to 3°C, and for the total change between 1983-2013 and 2069-2099.
 486 The warming sensitivity is based on [CO₂] held constant at the 2015 level but includes changes in other
 487 climate variables. The CO₂ sensitivity (e, f) in GC5 and GC6 is shown at specific [CO₂] concentrations and
 488 for the 2069-2099 mean concentrations. Warming and CO₂ sensitivities are calculated based on crop model
 489 responses over a 21-year window centered on the year in which a certain temperature change or [CO₂]
 490 concentration occurs in each climate model. Filled circles indicate the median crop model response,

491 additionally highlighted by circled numbers underneath each plot. Black bars show the inter-quartile range
 492 and individual models are indicated by numbers. Note that both panel **c** and **d** include two different legends.
 493 See Figure S7 for soybean and rice results. ACEA and DSSAT-Pythia have not submitted simulations for
 494 the constant [CO₂] setting and are excluded from panel **c-f**.
 495
 496
 497
 498
 499



500

501 **Fig. 8: Variance decomposition of ensemble projections.** Stacks show the fraction of total variance of
 502 mid-century crop production changes (2030-2070 mean) induced by the climate model ensemble (GCMs;
 503 yellow) and by the crop model ensemble (GGCMs; pink), for GGCMi-CMIP6 (GC6) and GGCMi-CMIP5
 504 (GC5), respectively. Variance fractions are normalized by the variance cross term to be additive. The
 505 absolute variance introduced by GGCMs and GCMs is indicated at the base of each stack. The GCM
 506 ensemble has 5 members in both cases, the GGCM ensemble has 12 members in GC6 and 7 members in
 507 GC5, which further highlights that the crop model response became more consistent in GC6 compared to
 508 the climate model uncertainty.

509 Methods

510 Time of emergence metric

511 We define Time of Climate Impact Emergence (TCIE) as the year in which the smoothed climate
512 change signal ('signal') exceeds the underlying internal variability and model uncertainty ('noise'). The
513 signal is the multi-model ensemble mean crop productivity change against the 1983-2013 reference
514 period (smoothed with a 25-yr moving window). Noise is defined as the standard deviation of simulated
515 historical variability of crop productivity across all individual GCM x GGCM combinations (1983-2013).
516 TCIE is the first year in which the signal emerges from the noise, i.e., when the signal-to-noise ratio
517 becomes greater than 1. Similar time of emergence definitions have been used in previous
518 studies^{e.g.10,13,68,69}. Historical productivity time series are not detrended as we hold all management
519 factors constant throughout the simulations. To assess TCIE uncertainties, we calculate TCIE also for
520 each individual climate-crop model realization as suggested by Hawkins and Sutton 2012¹², and we
521 analyze the distribution of the individual estimates (including mean, median, inter-quartile range, and
522 SD). We find that the multi-model ensemble mean TCIE usually occurs between the median and the
523 mean of individual TCIE estimates. For example, global-level maize production under RCP8.5 shows a
524 multi-model ensemble mean TCIE in year 2032, the median of individual estimates occurs in year 2027,
525 the mean in year 2036. Wheat shows the same pattern and results are qualitatively the same across
526 the different methods. To test the robustness of results in another way, we calculate the multi-model
527 ensemble mean TCIE iteratively while removing one crop model at a time. The SD of this distribution at
528 global level is marginal; 1.5 years for both maize and wheat under RCP8.5. As a final metric, we also
529 compare the number of climate and crop model combinations that show an emergence signal by the
530 end of the century. We calculate TCIE at global level, for different Koeppen-Geiger climate zones, and
531 for individual grid cells. Earlier TCIE is generally found for larger spatial scales as the variance of
532 internal variability decreases with averaging. For additional discussions see for example references¹¹⁻
533 ¹³.

534 ISIMIP climate input datasets

535 GGCM simulation efforts for CMIP6 impact assessment are aligned with the ISIMIP³ activity in which
536 GGCM represents the agriculture sector. Key modeling inputs such as information on climate, land
537 use, fertilizer input, soils, among others, are harmonized across various research sectors. CMIP6
538 climate model outputs are centrally bias-adjusted and downscaled by the ISIMIP framework to provide
539 climate-input datasets on a daily regular 0.5°x0.5° global grid. The bias-adjustment method employs a
540 quantile mapping approach and uses the observational W5E5 v1.0 dataset^{67,68}. This historical dataset
541 compares favorably with climatic forcing datasets that have been used previously by AgMIP GGCM⁶⁹.
542 The new quantile-mapping method adjusts biases and preserves trends in all quantiles of the
543 distribution of simulated daily climate model outputs; for more details see Lange (2019)¹⁰. To lower the
544 barrier for participation in this study we provide climate input data for five CMIP6 GCMs: GFDL-ESM4,
545 IPSL-CM6A-LR, MPI-ESM1-2-HR, MRI-ESM2-0, UKESM1-0-LL (see Table S1 for further details). The
546 GCM selection is based on data availability at the time of selection, performance in the historical period,
547 structural independence, process representation and equilibrium climate sensitivity (ECS). The five
548 GCMs are structurally independent in terms of their ocean and atmosphere model components and
549 overall they represent the range of ECS across the full CMIP6 ensemble, including three models with
550 below-average ECS (GFDL-ESM4, MPI-ESM1-2-HR, MRI-ESM2-0) and two models with above-
551 average ECS (IPSL-CM6A-LR, UKESM1-0-LL)⁸. ECS and transient climate response (TCR) for all
552 GCMs used are listed in Table S1. The mean and standard deviation (SD) of both ECS (mean = 3.7°C,
553 SD = 1.1) and TCR (mean = 2.0°C, SD = 0.5) across the five GCMs used here precisely match the
554 mean and SD across the full CMIP6 ensemble with 38 members (Table S1 and S2), much better than
555 in GC5, although the range of ECS in the CMIP6 ISIMIP models is larger than in the CMIP5 ISIMIP
556 models.

557

558 The daily weather variables at a 0.5° spatial resolution that are used as input for the crop models
559 include: daily mean, minimum, and maximum 2-m air temperature (T, Tmin, and Tmax, respectively

560 [°C]), daily total precipitation (P [mm]), and daily mean shortwave and longwave radiation (SR and LR
561 [W/m²]).

562 GGCM Phase 3 crop modeling protocol

563 Bias-adjusted climate model projections are used to drive transient crop model simulations, i.e.,
564 uninterrupted runs for the historical (1850-2014), and future (2015-2100) time period. Potential future
565 trajectories are represented by SSP1 with RCP2.6 (here SSP126) and SSP5 with RCP8.5 (here
566 SSP585). Therefore, each crop model performs 20 future simulation runs for each crop (5 GCM x 2
567 RCP x 2 [CO₂] settings). Note that in this study any socio-economic forcing or adaptation effort
568 associated with the SSP storylines is held constant at the year 2015 level to isolate the climate signal
569 (i.e., year 2015 land-use, fertilizer application, growing seasons, crop cultivars, but also NO₃ and NH₄
570 deposition rates, are used in years after 2015). To help isolate yield effects associated with the CO₂
571 fertilization effect, all crop model simulations are run for two separate assumptions: i) transient [CO₂] in
572 line with the respective RCP ('default [CO₂]'), and ii) [CO₂] concentration held constant at the 2015 level
573 at 399.95 ppmv ('constant [CO₂]'). Differences between the two [CO₂] levels are not a measure of [CO₂]
574 uncertainty, as there is no plausible climate change scenario without increasing [CO₂]²². Instead, this
575 setup is used to quantify the size of the CO₂ fertilization effect. All simulations are carried out at the 0.5°
576 global grid. In addition to the GCM forcing, we include historical simulations based on the reanalysis
577 product GSWP3-W5E5 v1.0^{67,68} for each crop model and crop to better evaluate crop model
578 performance against observational data.

579

580 We focus on the four major global grain crops, that is, maize (*Zea mays L.*), wheat (*Triticum sp. L.*), rice
581 (*Oryza sativa L.*), and soybean (*Glycine max L. Merr.*). Wheat is simulated as winter and spring wheat
582 individually; grain and silage maize are not distinguished. These four main crops contribute 90% of
583 today's global caloric production of all cereals and soybean⁷⁰.

584

585 All crops are simulated under both rainfed conditions and full irrigation (where soil moisture is set to
586 field capacity every day, without constraints to water availability) in all grid cells — independent of the
587 current cropland distribution. The physical cropland extent is applied in post-processing based on the
588 MIRCA2000 (Monthly Irrigated and Rainfed Crop Areas around the year 2000) reference dataset⁷¹ and
589 irrigated fractions are adapted from Siebert et al. (2015)⁷²; both are held constant over time.

590

591 Soil moisture and soil temperature for various soil layers are calculated by most crop models in a
592 transient way, that is, without reinitializing at the beginning of each year. All models use a classic
593 phenological heat sum approach to determine physiological stages between planting and maturity. Heat
594 unit accumulation can be modified by the sensitivity to day length (photoperiod) and for winter wheat it
595 is stalled until vernalization requirements are reached, that is, the exposure to cold temperatures before
596 anthesis. Planting dates (see section ‘Crop calendar and crop varieties’ below) are constant over time
597 but the heat sum approach leads to different growing season lengths depending on the daily
598 temperature distribution in each growing season. Except for rice, we simulate only one growing season
599 per calendar year. The first and last years of the transient runs are removed from crop model
600 simulations due to partially incomplete growing seasons. Simulations in grid cells with a growing
601 season length less than 50 days are removed, as are simulations resulting in premature harvest (i.e.,
602 accumulated heat units <80% of required heat units and applies only to those models that can provide
603 such outputs).

604

605 The harmonization of crop models includes the required use of a central crop calendar product (new
606 development for this study, see below), fertilizer inputs, and soil information. Additional protocol
607 characteristics are recommended but not required, as not all models can address all features (see
608 below).

609

610 Simulation protocols determine mineral and organic fertilizer [kg N/ha] inputs per crop and grid cell.

611 Mineral fertilizer (ammonium nitrate; NH_4NO_3) application is crop-specific and is derived from the LUH2

612 product^{73,74}, harmonized by ISIMIP. Manure application inputs (C:N ratio of 14.5) are grid cell specific,
613 but constant across crops⁷⁵. All other nutrients are considered non-limiting. Fertilizer scheduling follows
614 a simple assumption with 20% applied at sowing and 80% applied when 25% of the heat units required
615 to reach maturity are accumulated. As all other management aspects, fertilizer application is held
616 constant throughout the simulation period. Atmospheric N deposition is considered, separating NH_x and
617 NO_y, based on Tian et al. (2018)⁷⁶ and held constant at the year 2015 level.

618

619 Soil input is harmonized across crop models for the first time in GGCM, derived from the Harmonized
620 World Soil Database (HWSD)⁷⁷. While the same HWSD dataset is used across ISIMIP sectors, in this
621 study we employ a different algorithm to aggregate the data to 0.5° in order to be cropland specific. The
622 pDSSAT model uses the Global Soil Data set for Earth system modeling (GSDE)⁷⁸ and DSSAT-Pythia
623 uses the Global High-Resolution Soil Profile Database for Crop Modeling Applications⁷⁹ due to
624 difficulties in retrieving all soil parameters from HWSD.

625

626 Finally, the following management aspects are encouraged to be harmonized across crop models, but
627 are not accounted for by all teams: tillage (2 tillage events, planting day and harvest day, 200 mm
628 depth, full inversion), residues (70% of above-ground residues removed), no pest and disease damage,
629 no soil erosion, and no cover crops. Except for rice and wheat, which are simulated for two separate
630 growing seasons, we do not consider multi-cropping systems or crop rotations. Inputs are provided for
631 18 different crops globally, but most crop models can only simulate the major crops, which we focus on
632 in this study. All socio-economic and farm management input data are publicly available via
633 www.isimip.org.

634 Participating GGCM crop models

635 Twelve process-based global crop models participate in this study: ACEA, CROVER, CYGMA1p74,
636 DSSAT-Pythia, EPIC-IIASA, ISAM, LandscapeDNDC, LPJmL, pDSSAT, PEPIC, PROMET,
637 SIMPLACE-LINTUL5 (see Table S3 for further details and references). The full ensemble, therefore,

638 consists of roughly 240 future crop model simulations per crop plus one historical reference run for
639 each crop and climate model and one historical reanalysis run per crop model. Due to computational
640 constraints, ACEA has only run GCMs UKESM1-0-LL and MRI-ESM2-0 so far, and DSSAT-Pythia has
641 not yet run UKESM1-0-LL. ACEA and DSSAT-Pythia have not yet finished simulations for the constant
642 [CO₂] setting.

643
644 All crop models are considered independent. LPJmL, pDSSAT, EPIC-IIASA, PROMET, and PEPIC
645 have participated in previous GGCM protocols^{7,80-82}, and while the other models are new GGCM
646 ensemble members, they have been thoroughly evaluated individually (see references in Table S3). In
647 order to participate in this study, each model was required to go through a benchmark performance
648 evaluation for the historical period based on GSWP3-W5E5 reanalysis data (results available upon
649 request). An overview of the degree to which the GC6 crop models explain observed inter-annual yield
650 variability is presented in Figure S11. For the top five producer countries per crop, the ensemble mean
651 generally shows higher performance in terms of correlation and root-mean-square error than the bulk of
652 individual models. Generally, explained variability in individual models is satisfactory for most maize,
653 wheat, and soybean main-producer countries. The metrics are lower for rice which also links to the fact
654 that the weather signal in (largely irrigated) rice is smaller than in other crops, and the overall observed
655 inter-annual variability in these rice producer countries is smaller than for the other crops. Since
656 management decisions (planting dates, crop rotations and areas, fertilizer application, irrigation, etc.)
657 are held constant over time, the crop models can only capture the interannual weather signal in
658 reported yields, which in general is much smaller in the tropics compared to mid- to high-latitude
659 regions. Additional in-depth GGCM model comparison and evaluation is presented by Müller et al.
660 (2017)⁸¹. Overall, crop model performance evaluation based on historical yield variability provides
661 limited insight into the models' capability to project future yield impacts⁸³.

662
663 Since GCM-based crop model simulations are difficult to compare with observed inter-annual yield
664 levels (e.g., the 1988 drought does not necessarily occur in 1988 in the GCM), we compare the overall

665 range of simulated and observed yield variability across the historical reference period. The standard
666 deviation of observed national yield variability is matched to a substantially higher degree in GC6 (R =
667 79%, RMSE = 0.11) than in GC5 (R = 44%, RMSE = 0.17), which is indicative of more realistic yield
668 responses in GC6 (Fig. S10). These improvements are linked to a combination of factors, including
669 different internal variability in CMIP6, new GCM bias-adjustment method, improved crop model
670 ensemble, new crop yield bias-correction, and improved crop model inputs. The match with observed
671 yield variability using GC6 simulations based on GSWP3-W5E5 reanalysis data is only slightly better (R
672 = 87%, RMSE = 0.09) than with GCM-forced simulations, which highlights that the CMIP6 GCMs do not
673 introduce substantial errors in terms of historical variability (Fig. S10).

674
675 While the models generally reproduce yield declines in extreme years, adverse impacts of excess water
676 on crop growth due to lower aeration, waterlogging, and nitrogen leaching are generally
677 underrepresented in current global crop models³⁹. As an exception, the crop model CYGMA accounts
678 for effects due to excess moisture stress⁸⁴. ACEA, EPIC-based, and DSSAT-based crop models also
679 have processes related to waterlogging and root aeration but associated stresses occur rarely and
680 foremost on sensitive soils⁸⁵. Many models do not handle direct effects of extreme heat (e.g., on leaf
681 senescence, pollen sterility; see Table S3)³. Individual model responses to elevated [CO₂] are shown in
682 Figure 7 and S8 and discussed in the main text. The ISAM model requires sub-daily weather data and
683 therefore uses CRU–National Centers for Environmental Prediction (CRUNCEP) diurnal factors to
684 convert daily bias-adjusted climate model data to diurnal data. The PROMET model also requires sub-
685 daily weather data and uses ERA5-derived diurnal factors to convert climate model data to diurnal
686 inputs; it also uses WFDE5 instead of GSWP3-W5E5 for reanalysis simulations.

687
688 All models use spin-up simulations of various lengths to reach soil and carbon pool equilibrium. EPIC-
689 IIASA uses dynamic soil handling during spin-up to generate soil attributes. Subsequently these are
690 used as an input in the actual simulations with static soil handling, i.e. annual re-initialization of all soil
691 attributes (including soil organic matter fractions and soil texture among others) except mineral nutrient

692 pools, temperature, and soil moisture. The models do not account for human management intervention
693 other than fertilizer application, irrigation, seed selection, growing periods, and basic field management
694 such as tillage and residue removal.

695

696 All models follow a phenology calibration with respect to grid cell-specific cultivar parameterizations
697 (i.e., phenological heat units) based on the respective crop calendar and weather forcing (Table S3).
698 Yield calibration is not harmonized across crop models and each team follows their individual protocol,
699 including grid cell-specific calibration against SPAM⁸⁶ reference yields (e.g., pDSSAT), various site-
700 specific efforts based on field experiments (e.g., ISAM), and calibrations with national FAO⁷⁰ statistics
701 (e.g., PEPIC).

702 Crop yield bias correction

703 Crop production is calculated as yield times harvested area of the respective crop. We omit grid cells
704 with <10 ha cropland area for each crop. To compare results across crop models, but also to represent
705 realistic overall crop production estimates and spatial pattern, we calculate fractional yield changes
706 from each individual crop model simulation between the historical reference period (1983-2013) and the
707 respective future projection and multiply these with a spatially explicit (0.5°) observational yield
708 reference dataset (see Fig. S14 in ref.⁸⁷). SPAM2005 (Spatial Production Allocation Model 2005)⁸⁸ is
709 used as the main reference yield data as it separates rainfed and irrigated systems. Grid cells with
710 missing SPAM2005 yield data but with >10 ha MIRCA2000 harvested area are gap-filled with Ray et al.
711 (2012)⁸⁹ yield data; both SPAM2005 and Ray et al. represent the time period 2003 to 2007.

712 Winter and spring wheat separation

713 While winter and spring wheat are simulated separately by the crop models covering all land areas, our
714 analyses distinguish winter and spring wheat harvested areas using a rule-based approach. We
715 assume that winter wheat is grown in a specific grid cell if: i) the average temperature of the coldest
716 month is between -10°C and +7°C, ii) the growing season length exceeds 150 days, and iii) the growing

717 season includes December (Northern Hemisphere) or July (Southern Hemisphere). These assumptions
718 are slightly modified from the rule set in MIRCA2000⁷¹; we use 7°C instead of 6°C as the upper
719 temperature threshold to allow for more winter wheat in Argentina, South Africa, and Australia, but also
720 to extend winter wheat in the US slightly towards the south (Fig. S12). This modification is done to
721 better represent the winter wheat mega environments used by CIMMYT⁹⁰. The winter and spring wheat
722 rule set is also used to separate wheat crop calendars in case the two are not distinguished in the
723 original crop calendar data. In line with other cropland areas as well, winter and spring wheat areas are
724 held constant over time.

725 Crop calendar and crop varieties

726 We provide planting and maturity dates for each crop in each grid cell, separate for rainfed and irrigated
727 systems, based on a new observational crop calendar product. See section 'GGCMI crop calendar' and
728 Fig. S13-S15 in the Supplement for details. Growing season inputs are static over time throughout the
729 historical and future time period to avoid confounding trends. Each model calculated required reference
730 heat units to reach physiological maturity for each crop in each grid cell by averaging annual heat sums
731 over all growing seasons between 1979-2010.

732 Koeppen-Geiger climate class aggregation

733 Koeppen-Geiger climate zones⁹¹ are aggregated to 0.5° spatial resolution and the 32 individual classes
734 are aggregated to the following four main climate types: temperature-limited
735 ("Dfc", "Dfd", "Dsc", "Dsd", "Dwc", "Dwd", "ET", "EF", "H", "BSk"), temperate/humid
736 ("Csb", "Cfa", "Cfb", "Cfc", "Csc", "Cwa", "Cwb", "Cwc", "Dfa", "Dfb", "Dsa", "Dsb", "Dwa", "Dwb"),
737 subtropical/Mediterranean ("Csa", "BSh", "Af", "Am", "As", "Aw"), and tropical/other (all other classes).

738 Map projection and smoothing

739 Global maps are based on the Robinson projection⁹² and grid-level data are smoothed to improve
740 clarity and visual appearance. Smoothing is done by first resampling the raw data to 5 times finer

741 resolution, followed by a 5x5 grid cell focal mean window aggregation. Map smoothing is done for
742 visualization purposes only and all analyses are based on the raw data.

743 Acknowledgements

744 J.J., A.C.R., C.R., and M.P.P. were supported by NASA GISS Climate Impacts Group and Indicators for
745 the National Climate Assessment funding from the NASA Earth Sciences Division. J.J. received support
746 from the Open Philanthropy Project and thanks the University of Chicago Research Computing Center
747 for supercomputer allocations to run the pDSSAT model. Ludwig-Maximilians-Universität München
748 thanks the Leibniz Supercomputing Center of the Bavarian Academy of Sciences and Humanities for
749 providing capacity on the Cloud computing infrastructure to run the PROMET model. J.M.S. was
750 supported by the German Federal Ministry of Education and Research (grant-number 031B0230A:
751 BioNex—The Future of the Biomass Nexus). O.M. and J.F.S. were supported by funding from the
752 European Research Council (ERC) under the European Union’s Horizon 2020 research and innovation
753 programme (Earth@lternatives project, grant agreement No 834716). J.A.F. and H.S. were supported
754 by the NSF NRT program (grant no. DGE-1735359). J.A.F. was supported by the NSF Graduate
755 Research Fellowship Program (grant no. DGE-1746045). RDCEP is funded by NSF through the
756 Decision Making Under Uncertainty program (grant #SES-1463644). T.I. was partly supported by the
757 Environment Research and Technology Development Fund (2-2005) of the Environmental Restoration
758 and Conservation Agency and Grant-in-Aid for Scientific Research B (18H02317) of the Japan Society
759 for the Promotion of Science. M.O. was supported by the Climate Change Adaptation Research
760 Program of NIES, Japan. S.L. was supported by the German Federal Office for Agriculture and Food
761 (BLE) in the framework of OptAKlim (grant no. 281B203316). S.R. acknowledges funding from the
762 German Federal Ministry of Education and Research (BMBF) via the ISlpedia project.

763 Author contributions

764 J.J. and C.M. conceived the paper and coordinate GGCM. J.J., C.M., and S.R. developed the
765 simulation protocol. A.R. and C.R. coordinate AgMIP integration. C.M., J.J., J.B., O.C., B.F., C.F., K.F.,
766 G.H. T.I., A.J. N.K, T.L., W.L., S.M., M.O., O.M., C.P. S.R., J.S., J.S. R.S., A.S., T. S., F.Z. conducted
767 crop model simulations, S.L. prepared climate data inputs, J.J. developed the manuscript and figures,
768 all coauthors supported writing and discussion of the results.

769 Data and materials availability

770 All data needed to evaluate the conclusions in the paper are present in the paper and/or the
771 Supplementary Materials. Model inputs are publicly available via <https://www.isimip.org/> or from the
772 corresponding author. Crop model simulations will be made public under the CC0 license pending
773 publication.

774
775 The authors declare no competing interest. This article contains supporting information online.

776 References

777 1. Mbow, C. *et al.* Food security. in *Climate Change and Land: an IPCC special report on climate*
778 *change, desertification, land degradation, sustainable land management, food security, and*

- 779 *greenhouse gas fluxes in terrestrial ecosystems* **1**, 270 (2019).
- 780 2. Asseng, S. *et al.* Uncertainty in simulating wheat yields under climate change. *Nat. Clim. Chang.*
781 **3**, 827–832 (2013).
- 782 3. Wang, E. *et al.* The uncertainty of crop yield projections is reduced by improved temperature
783 response functions. *Nat. Plants* **3**, (2017).
- 784 4. Rosenzweig, C. *et al.* The Agricultural Model Intercomparison and Improvement Project (AgMIP):
785 Protocols and pilot studies. *Agric. For. Meteorol.* **170**, 166–182 (2013).
- 786 5. ISIMIP. The Inter-Sectoral Impact Model Intercomparison Project. 2021 Available at:
787 <https://www.isimip.org/>.
- 788 6. Eyring, V. *et al.* Overview of the Coupled Model Intercomparison Project Phase 6 (CMIP6)
789 experimental design and organization. *Geosci. Model Dev.* **9**, 1937–1958 (2016).
- 790 7. Rosenzweig, C. *et al.* Assessing agricultural risks of climate change in the 21st century in a
791 global gridded crop model intercomparison. *Proc. Natl. Acad. Sci.* **111**, 3268–3273 (2014).
- 792 8. Meehl, G. A. *et al.* Context for interpreting equilibrium climate sensitivity and transient climate
793 response from the CMIP6 Earth system models. *Sci. Adv.* **6**, 1–11 (2020).
- 794 9. O’Neill, B. C. *et al.* The Scenario Model Intercomparison Project (ScenarioMIP) for CMIP6.
795 *Geosci. Model Dev.* **9**, 3461–3482 (2016).
- 796 10. Lange, S. Trend-preserving bias adjustment and statistical downscaling with ISIMIP3BASD
797 (v1.0). *Geosci. Model Dev.* **12**, 3055–3070 (2019).
- 798 11. Hawkins, E. *et al.* Observed Emergence of the Climate Change Signal: From the Familiar to the
799 Unknown. *Geophys. Res. Lett.* **47**, (2020).
- 800 12. Hawkins, E. & Sutton, R. Time of emergence of climate signals. *Geophys. Res. Lett.* **39**, 1–6
801 (2012).
- 802 13. Kirtman, B. *et al.* Near-term climate change: Projections and predictability. *Clim. Chang.* 2013
803 *Phys. Sci. Basis Work. Gr. I Contrib. to Fifth Assess. Rep. Intergov. Panel Clim. Chang.*
804 **9781107057**, 953–1028 (2013).
- 805 14. Seneviratne, S. I. & Hauser, M. Regional Climate Sensitivity of Climate Extremes in CMIP6
806 Versus CMIP5 Multimodel Ensembles. *Earth’s Futur.* **8**, 1–12 (2020).
- 807 15. Rojas, M., Lambert, F., Ramirez-Villegas, J. & Challinor, A. J. Emergence of robust precipitation
808 changes across crop production areas in the 21st century. *Proc. Natl. Acad. Sci.* **116**, 6673–
809 6678 (2019).
- 810 16. Raymond, C., Matthews, T. & Horton, R. M. The emergence of heat and humidity too severe for
811 human tolerance. *Sci. Adv.* **6**, (2020).
- 812 17. Park, C. E. *et al.* Keeping global warming within 1.5 °c constrains emergence of aridification. *Nat.*
813 *Clim. Chang.* (2018). doi:10.1038/s41558-017-0034-4
- 814 18. Liu, B. *et al.* Similar estimates of temperature impacts on global wheat yield by three

- 815 independent methods. *Nat. Clim. Chang.* **6**, 1130–1136 (2016).
- 816 19. Zhao, C. *et al.* Plausible rice yield losses under future climate warming. *Nat. Plants* **3**, 1–5
817 (2016).
- 818 20. Zhao, C. *et al.* Temperature increase reduces global yields of major crops in four independent
819 estimates. *Proc. Natl. Acad. Sci.* 201701762 (2017). doi:10.1073/pnas.1701762114
- 820 21. Deryng, D. *et al.* Regional disparities in the beneficial effects of rising CO₂ concentrations on
821 crop water productivity. *Nat. Clim. Chang.* (2016). doi:10.1038/nclimate2995
- 822 22. Ruane, A. C. *et al.* Biophysical and economic implications for agriculture of +1.5° and +2.0°C
823 global warming using AgMIP Coordinated Global and Regional Assessments. *Clim. Res.* **76**, 17–
824 39 (2018).
- 825 23. Ahmed, M. *et al.* Novel multimodel ensemble approach to evaluate the sole effect of elevated
826 CO₂ on winter wheat productivity. *Sci. Rep.* **9**, 1–15 (2019).
- 827 24. Leakey, A. D. B., Bishop, K. A. & Ainsworth, E. A. A multi-biome gap in understanding of crop
828 and ecosystem responses to elevated CO₂. *Current Opinion in Plant Biology* (2012).
829 doi:10.1016/j.pbi.2012.01.009
- 830 25. Toreti, A. *et al.* Narrowing uncertainties in the effects of elevated CO₂ on crops. *Nat. Food* **1**,
831 775–782 (2020).
- 832 26. Hausfather, Z. & Peters, G. P. Emissions – the ‘business as usual’ story is misleading. *Nature*
833 **577**, 618–620 (2020).
- 834 27. Minoli, S. *et al.* Global Response Patterns of Major Rainfed Crops to Adaptation by Maintaining
835 Current Growing Periods and Irrigation. *Earth’s Futur.* **7**, 1464–1480 (2019).
- 836 28. Wang, X. *et al.* Emergent constraint on crop yield response to warmer temperature from field
837 experiments. *Nat. Sustain.* **3**, 908–916 (2020).
- 838 29. Asseng, S. *et al.* Rising temperatures reduce global wheat production. *Nat. Clim. Chang.* **5**, 143–
839 147 (2014).
- 840 30. Kimball, B. A. Crop responses to elevated CO₂ and interactions with H₂O, N, and temperature.
841 *Current Opinion in Plant Biology* (2016). doi:10.1016/j.pbi.2016.03.006
- 842 31. Zabel, F. *et al.* Large potential for crop production adaptation depends on available future
843 varieties. *Glob. Chang. Biol.* gcb.15649 (2021). doi:10.1111/gcb.15649
- 844 32. Ray, D. K. *et al.* Climate change has likely already affected global food production. *PLoS One*
845 **14**, 1–18 (2019).
- 846 33. Lobell, D. B., Schlenker, W. & Costa-Roberts, J. Climate trends and global crop production since
847 1980. *Science* **333**, 616–20 (2011).
- 848 34. Ahmad, S. *et al.* Climate warming and management impact on the change of phenology of the
849 rice-wheat cropping system in Punjab, Pakistan. *F. Crop. Res.* **230**, 46–61 (2019).
- 850 35. Porter, J. R. *et al.* Food security and food production systems. in *Climate Change 2014: Impacts,*

- 851 *Adaptation, and Vulnerability. Part A: Global and Sectoral Aspects. Contribution of Working*
852 *Group II to the Fifth Assessment Report of the Intergovernmental Panel on Climate Change*
853 (eds. Field, C. B. et al.) 485–533 (Cambridge University Press, 2014).
- 854 36. Levis, S., Badger, A., Drewniak, B., Nevison, C. & Ren, X. CLMcrop yields and water
855 requirements: avoided impacts by choosing RCP 4.5 over 8.5. *Clim. Change* **146**, 501–515
856 (2018).
- 857 37. Falconnier, G. N. et al. Modelling climate change impacts on maize yields under low nitrogen
858 input conditions in sub-Saharan Africa. *Glob. Chang. Biol.* **26**, 5942–5964 (2020).
- 859 38. O’Neill, B. C. et al. IPCC reasons for concern regarding climate change risks. *Nat. Clim. Chang.*
860 **7**, 28–37 (2017).
- 861 39. Li, Y., Guan, K., Schnitkey, G. D., DeLucia, E. & Peng, B. Excessive rainfall leads to maize yield
862 loss of a comparable magnitude to extreme drought in the United States. *Glob. Chang. Biol.* **25**,
863 2325–2337 (2019).
- 864 40. Zhu, P., Zhuang, Q., Archontoulis, S. V., Bernacchi, C. & Müller, C. Dissecting the nonlinear
865 response of maize yield to high temperature stress with model-data integration. *Glob. Chang.*
866 *Biol.* **25**, 2470–2484 (2019).
- 867 41. Christensen, J. H. et al. Regional Climate Projections. in *Climate Change 2007: The Physical*
868 *Science Basis. Contribution of Working Group I to the Fourth Assessment Report of the*
869 *Intergovernmental Panel on Climate Change* (ed. Solomon, S., D. Qin, M. Manning, Z. Chen, M.
870 Marquis, K.B. Averyt, M. T. and H. L. M.) 11–15 (Cambridge University Press, 2007).
871 doi:10.1007/978-81-322-1967-5_4
- 872 42. Iizumi, T. et al. Responses of crop yield growth to global temperature and socioeconomic
873 changes. *Sci. Rep.* **7**, 1–10 (2017).
- 874 43. Sherwood, S. C. et al. An Assessment of Earth’s Climate Sensitivity Using Multiple Lines of
875 Evidence. *Rev. Geophys.* **58**, 1–92 (2020).
- 876 44. Flynn, C. M. & Mauritsen, T. On the climate sensitivity and historical warming evolution in recent
877 coupled model ensembles. *Atmos. Chem. Phys.* **20**, 7829–7842 (2020).
- 878 45. Zelinka, M. D. et al. Causes of Higher Climate Sensitivity in CMIP6 Models. *Geophys. Res. Lett.*
879 **47**, 1–12 (2020).
- 880 46. Tokarska, K. B. et al. Past warming trend constrains future warming in CMIP6 models. *Sci. Adv.*
881 **6**, 1–14 (2020).
- 882 47. Williams, K. D., Hewitt, A. J. & Bodas-Salcedo, A. Use of Short-Range Forecasts to Evaluate
883 Fast Physics Processes Relevant for Climate Sensitivity. *J. Adv. Model. Earth Syst.* **12**, 1–9
884 (2020).
- 885 48. Brunner, L. et al. Reduced global warming from CMIP6 projections when weighting models by
886 performance and independence. *Earth Syst. Dyn.* **11**, 995–1012 (2020).

- 887 49. Nijse, F. J. M. M., Cox, P. M. & Williamson, M. S. Emergent constraints on transient climate
888 response (TCR) and equilibrium climate sensitivity (ECS) from historical warming in CMIP5 and
889 CMIP6 models. *Earth Syst. Dyn.* **11**, 737–750 (2020).
- 890 50. Ridder, N. N., Pitman, A. J. & Ukkola, A. M. Do CMIP6 Climate Models simulate Global or
891 Regional Compound Events skilfully? *Geophys. Res. Lett.* 1–11 (2020).
892 doi:10.1029/2020gl091152
- 893 51. Fan, X., Miao, C., Duan, Q., Shen, C. & Wu, Y. The Performance of CMIP6 Versus CMIP5 in
894 Simulating Temperature Extremes Over the Global Land Surface. *J. Geophys. Res. Atmos.* **125**,
895 1–16 (2020).
- 896 52. Xin, X., Wu, T., Zhang, J., Yao, J. & Fang, Y. Comparison of <sc>CMIP6</sc> and
897 <sc>CMIP5</sc> simulations of precipitation in China and the East Asian summer monsoon.
898 *Int. J. Climatol.* **40**, 6423–6440 (2020).
- 899 53. Meinshausen, M. *et al.* The shared socio-economic pathway (SSP) greenhouse gas
900 concentrations and their extensions to 2500. *Geosci. Model Dev.* **13**, 3571–3605 (2020).
- 901 54. Von Bloh, W. *et al.* Implementing the nitrogen cycle into the dynamic global vegetation,
902 hydrology, and crop growth model LPJmL (version 5.0). *Geosci. Model Dev.* **11**, 2789–2812
903 (2018).
- 904 55. Jägermeyr, J. & Frieler, K. Spatial variations in crop growing seasons pivotal to reproduce global
905 fluctuations in maize and wheat yields. *Sci. Adv.* **4**, eaat4517 (2018).
- 906 56. Müller, C. *et al.* Exploring uncertainties in global crop yield projections in a large ensemble of
907 crop models and CMIP5 and CMIP6 climate scenarios. *Environ. Res. Lett.* **16**, 034040 (2021).
- 908 57. Franke, J. A. *et al.* The GGCM Phase 2 emulators: global gridded crop model responses to
909 changes in CO₂, temperature, water, and nitrogen (version 1.0). *Geosci. Model Dev.* **13**, 2315–
910 2336 (2020).
- 911 58. Allen, L. H. *et al.* Fluctuations of CO₂ in Free-Air CO₂ Enrichment (FACE) depress plant
912 photosynthesis, growth, and yield. *Agric. For. Meteorol.* **284**, (2020).
- 913 59. Durand, J. L. *et al.* How accurately do maize crop models simulate the interactions of
914 atmospheric CO₂ concentration levels with limited water supply on water use and yield? *Eur. J.*
915 *Agron.* (2018). doi:10.1016/j.eja.2017.01.002
- 916 60. Myers, S. S. *et al.* Increasing CO₂ threatens human nutrition. *Nature* **510**, 139–42 (2014).
- 917 61. Zhu, C. *et al.* Carbon dioxide (CO₂) levels this century will alter the protein, micronutrients, and
918 vitamin content of rice grains with potential health consequences for the poorest rice-dependent
919 countries. *Sci. Adv.* **4**, eaaq1012 (2018).
- 920 62. Köhler, I. H., Huber, S. C., Bernacchi, C. J. & Baxter, I. R. Increased temperatures may
921 safeguard the nutritional quality of crops under future elevated CO₂ concentrations. *Plant J.* **97**,
922 872–886 (2019).

- 923 63. Rising, J. & Devineni, N. Crop switching reduces agricultural losses from climate change in the
924 United States by half under RCP 8.5. *Nat. Commun.* **11**, 4991 (2020).
- 925 64. Asseng, S. *et al.* Climate change impact and adaptation for wheat protein. *Glob. Chang. Biol.* **25**,
926 155–173 (2019).
- 927 65. Hawkins, E. & Sutton, R. The potential to narrow uncertainty in regional climate predictions. *Bull.*
928 *Am. Meteorol. Soc.* **90**, 1095–1107 (2009).
- 929 66. Giorgi, F. & Bi, X. Time of emergence (TOE) of GHG-forced precipitation change hot-spots.
930 *Geophys. Res. Lett.* **36**, L06709 (2009).
- 931 67. Lange, S. WFDE5 over land merged with ERA5 over the ocean (W5E5). V. 1.0. *GFZ Data*
932 *Services* (2019). doi:<https://doi.org/10.5880/pik.2019.023>
- 933 68. Cucchi, M. *et al.* WFDE5: Bias-adjusted ERA5 reanalysis data for impact studies. *Earth Syst.*
934 *Sci. Data* **12**, 2097–2120 (2020).
- 935 69. Ruane, A. C. *et al.* Strong regional influence of climatic forcing datasets on global crop model
936 ensembles. *Agric. For. Meteorol.* **300**, 108313 (2021).
- 937 70. FAO. FAOSTAT, United Nation’s Food and Agricultural Organization, Rome. (2019). Available
938 at: <http://www.fao.org/faostat/>. (Accessed: 10th July 2019)
- 939 71. Portmann, F. T., Siebert, S. & Döll, P. MIRCA2000 - Global monthly irrigated and rainfed crop
940 areas around the year 2000: A new high-resolution data set for agricultural and hydrological
941 modeling. *Global Biogeochem. Cycles* **24**, 1–24 (2010).
- 942 72. Siebert, S. *et al.* A global data set of the extent of irrigated land from 1900 to 2005. *Hydrol. Earth*
943 *Syst. Sci.* **19**, 1521–1545 (2015).
- 944 73. Mueller, N. D. *et al.* Closing yield gaps through nutrient and water management. *Nature* **490**,
945 254–7 (2012).
- 946 74. Hurtt, G. C. *et al.* Harmonization of global land use change and management for the period 850–
947 2100 (LUH2) for CMIP6. *Geosci. Model Dev.* **13**, 5425–5464 (2020).
- 948 75. Zhang, B. *et al.* Global manure nitrogen production and application in cropland during 1860–
949 2014: A 5 arcmin gridded global dataset for Earth system modeling. *Earth Syst. Sci. Data* **9**,
950 667–678 (2017).
- 951 76. Tian, H. *et al.* The Global N2O Model Intercomparison Project. *Bull. Am. Meteorol. Soc.* **99**,
952 1231–1251 (2018).
- 953 77. Nachtergaele, F. *et al.* Harmonized World Soil Database (version 1.2). *FAO, Rome, Italy IIASA,*
954 *Laxenburg, Austria* 1–50 (2012). doi:3123
- 955 78. Shangguan, W., Dai, Y., Duan, Q., Liu, B. & Yuan, H. A global soil data set for earth system
956 modeling. *J. Adv. Model. Earth Syst.* **6**, 249–263 (2014).
- 957 79. Hengl, T. *et al.* SoilGrids1km - Global soil information based on automated mapping. *PLoS One*
958 **9**, (2014).

- 959 80. Elliott, J. *et al.* The Global Gridded Crop Model Intercomparison: data and modeling protocols for
960 Phase 1 (v1.0). *Geosci. Model Dev.* **8**, 261–277 (2015).
- 961 81. Müller, C. *et al.* Global gridded crop model evaluation: benchmarking, skills, deficiencies and
962 implications. *Geosci. Model Dev.* **10**, 1403–1422 (2017).
- 963 82. Franke, J. A. *et al.* The GGCM Phase 2 experiment: global gridded crop model simulations
964 under uniform changes in CO₂, temperature, water, and nitrogen levels (protocol version 1.0).
965 *Geosci. Model Dev.* **13**, 2315–2336 (2020).
- 966 83. Ruane, A. C. *et al.* Multi-wheat-model ensemble responses to interannual climate variability.
967 *Environ. Model. Softw.* **81**, 86–101 (2016).
- 968 84. Wang, R., Bowling, L. C. & Cherkauer, K. A. Estimation of the effects of climate variability on
969 crop yield in the Midwest USA. *Agric. For. Meteorol.* **216**, 141–156 (2016).
- 970 85. Folberth, C., Gaiser, T., Abbaspour, K. C., Schulin, R. & Yang, H. Regionalization of a large-
971 scale crop growth model for sub-Saharan Africa: Model setup, evaluation, and estimation of
972 maize yields. *Agric. Ecosyst. Environ.* **151**, 21–33 (2012).
- 973 86. International Food Policy Research Institute. Global Spatially-Disaggregated Crop Production
974 Statistics Data for 2010 Version 1.0. *Harvard Dataverse V1* (2019). Available at:
975 <https://doi.org/10.7910/DVN/PRFF8V>. (Accessed: 15th February 2019)
- 976 87. Jägermeyr, J. *et al.* A regional nuclear conflict would compromise global food security. *Proc.*
977 *Natl. Acad. Sci.* **117**, 7071–7081 (2020).
- 978 88. International Food Policy Research Institute (IFPRI) & International Institute for Applied Systems
979 Analysis (IIASA). Global Spatially-Disaggregated Crop Production Statistics Data for 2005
980 Version 3.2. *Harvard Dataverse V9* (2016). Available at: <https://doi.org/10.7910/DVN/DHXBIX>.
981 (Accessed: 15th February 2019)
- 982 89. Ray, D. K., Ramankutty, N., Mueller, N. D., West, P. C. & Foley, J. a. Recent patterns of crop
983 yield growth and stagnation. *Nat. Commun.* **3**, 1293 (2012).
- 984 90. Reynolds, M. & Braun, H. Benefits to low-input agriculture. *Nat. Plants* **5**, 652–653 (2019).
- 985 91. Kottek, M., Grieser, J., Beck, C., Rudolf, B. & Rubel, F. World Map of the Köppen-Geiger climate
986 classification updated. *Meteorol. Zeitschrift* **15**, 259–263 (2006).
- 987 92. John P. Snyder & Voxland, P. M. *An album of map projections.* (1989). doi:10.3133/pp1453
988

Supplementary Files

This is a list of supplementary files associated with this preprint. Click to download.

- [SupplementJaegermeyretalNATFOOD20111649T.pdf](#)